

# We are IntechOpen, the world's leading publisher of Open Access books Built by scientists, for scientists

5,300

Open access books available

130,000

International authors and editors

155M

Downloads

Our authors are among the

154

Countries delivered to

TOP 1%

most cited scientists

12.2%

Contributors from top 500 universities



WEB OF SCIENCE™

Selection of our books indexed in the Book Citation Index  
in Web of Science™ Core Collection (BKCI)

Interested in publishing with us?  
Contact [book.department@intechopen.com](mailto:book.department@intechopen.com)

Numbers displayed above are based on latest data collected.  
For more information visit [www.intechopen.com](http://www.intechopen.com)



## Chapter

# Basic Volcanic Elements of the Arxan-Chaihe Volcanic Field, Inner Mongolia, NE China

*Boxin Li, Károly Németh, Julie Palmer, Alan Palmer, Jing Wu, Jonathan Procter and Jiaqi Liu*

## Abstract

The Arxan-Chaihe Volcanic Field, Inner Mongolia, NE China is a Pleistocene to Recent volcanic field still considered to be active. In this chapter we provide an update of current volcanological research conducted in the last four years to describe the volcanic architecture of the identified vents, their eruptive history and potential volcanic hazards. Here we provide an evidence-based summary of the most common volcanic eruption styles and types the field experienced in its evolution. The volcanic field is strongly controlled by older structural elements of the region. Hence most of the volcanoes of the field are fissure-controlled, fissure-aligned and erupted in Hawaiian to Strombolian-style creating lava spatter and scoria cone chains. One of the largest and most complex volcano of the field (Tongxin) experienced a violent phreatomagmatic explosive phase creating a maar in an intra-mountain basin, while the youngest known eruptions formed a triple vent set (Yanshan) that reached violent Strombolian phases and created an extensive ash and lapilli plains in the surrounding areas. This complex vent system also emitted voluminous lava flows that change the landscape by damming fluvial networks, providing a volcanological paradise for the recently established Arxan UNESCO Global Geopark.

**Keywords:** scoria, spatter, fissure, maar, tuff ring, pyroclastic density current, ash, tumuli, lava flow

## 1. Introduction

The Arxan-Chaihe Volcanic Field (ACVF) is a young intracontinental volcanic field located in the northeast of China (**Figure 1**). The volcanic field is best defined as a monogenetic volcanic field on the basis of the presence of small-volume volcanic edifices, eruptive products and typical landforms such as tuff rings, scoria (cinder) cones, fissure controlled vents, and complex, but small volcanic cones being the key elements of the volcano types preserved. Early research in the region focused on characterizing the volcanology of the area, however, in recent years research on the active volcanism in Northeast (NE) China has shed some light on magma genesis, volcanic edifice growth and volcanic hazards at some iconic locations such as the Changbaishan volcano, Longgang or Wudalianchi Volcanic Fields (**Figure 1**) [1]. This research has defined the basic characteristics of some of these

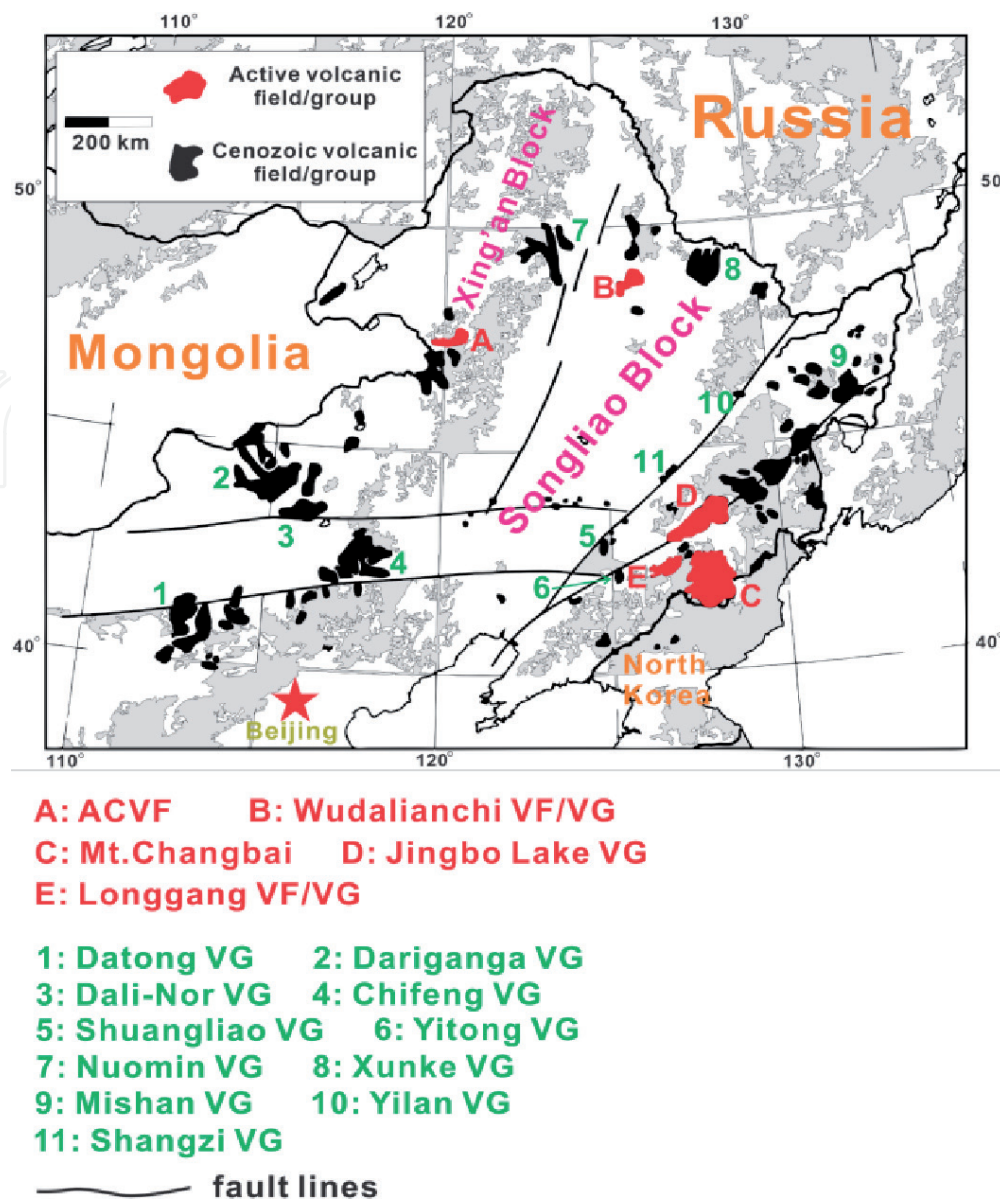


**Figure 1.**

*The general geological map of NE China: The red areas mark the active volcanic fields; the black areas indicate the ceased Cenozoic volcanic fields; also the solid lines in the territory of NE China are the markers of regional fault systems [1]. VF- volcanic field, VG – Volcanic group.*

volcanic regions, outlining the geochemical characteristics of the volcanic rocks and linking magma genesis to lithospheric processes. Volcanological research from NE. China are increasingly appearing in the international literature [2–8], however, there volcanic regions are largely unstudied. Among these is the Arxan-Chaihe Volcanic Field (ACVF). Several research outputs have made basic observations of the volcanic history of the region, but a systematic study has only recently been undertaken. Here we report a summary of volcanological observations made in the last six years of research on the ACVF. The aim of the study is to understand the eruptive history, volcanic stratigraphy, eruption styles and associated volcanic hazards that may be associated with the ACVF.

In this book chapter, we summarize the field-based observations of two major field campaigns to provide some basic descriptions of the recognized volcanic products including the most accessible and iconic volcanoes that form the core of the newly established Arxhan UNESCO Global Geopark [9]. We included Tongxin Lake on the northeast corner of ACVF, the Heaven Lake, Tuofengling Lake, Dichi Lake and Yanshan volcanic group (informally identified as the “Triple Vent”) (**Figure 2**) to

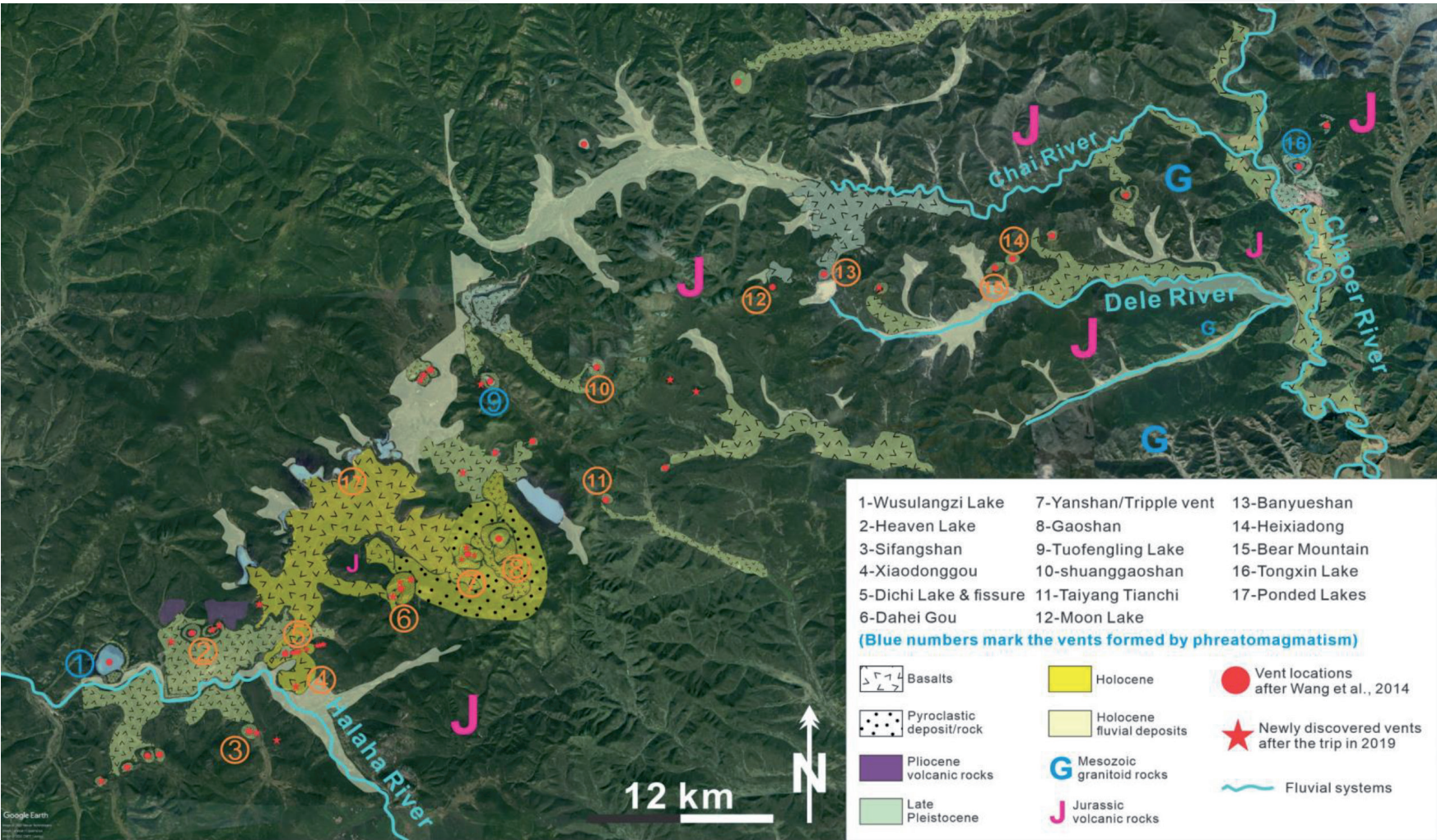


**Figure 2.** The map of vent distributions of ACVF (red dots) in relationship with the patterns indicating the distributions of volcanic eruptive products from previous research [10]. Numbers refer to locations mentioned in the text.

provide evidence of the important role of explosive hydrovolcanism, fissure-fed eruptions, Strombolian-style eruptions and various large-volume lava outpouring to the volcanic architecture of the field. We demonstrate that the Tongxin Lake near Chaihe township (**Figure 2**) is a tuff ring of explosive phreatomagmatic origin that covered an area of at least 13 km<sup>2</sup> (**Figure 2**). Eruptions from Tongxin Volcano were probably the most violent in the ACVF indicating the importance of externally-driven explosive hydrovolcanism during the eruptive history of ACVF. In contrast, the youngest known eruption site at Yanshan (C14–2040 +/-75; 1960 +/-70; 1990 +/-100; 1900 +/-70, BP) [11] is a nested scoria and spatter cone with three distinct vents forming a volcanic complex producing scoria-fall, agglutinated and clastogenic lavas. This location demonstrates probably the most common type of volcanic eruption in the ACVF. They are also the most voluminous and the youngest.

The region at and nearby Dichi Lake vent produced the smallest eruptive volumes in ACVF (**Figure 2**). The crater wall of Dichi Lake is composed of lava flows. These were disrupted by an explosive event that left produced angular breccias as a pyroclast ring around the now water-filled crater, best defined as a maar volcano. From Dichi Lake, however, a NE–SW trending fissure exposing a chain of vents gradually builds spatter cones and small scoria cones (**Figure 2**).

The majority of the volcanoes in the western side of the ACVF, closer to Arxan are clearly volcanoes that erupted through magmatic explosion and effusive processes and formed lava spatter cones, spatter ramparts, scoria cones and associated lava flows. Large, elongate craters in this region is filled by water, for example Tuofengling (**Figure 2**). Tuofengling was first interpreted as a scoria cone, but recent field mapping has revealed it is a complex volcanic cone with a basal tuff ring capped by a scoria cone complex. The field-based data presented here provide evidence of one of the largest Pleistocene phreatomagmatic explosive eruptions in the ACVF that formed a maar within a closed intramountain basin (**Figure 2**).

## 2. Geological setting

ACVF is located about 2000 km away from the Japan subduction zone (**Figure 1**). Thus, the background settings are generally under controls by intra-continental settings influenced by a distant convergent plate margin.

From the satellite map, ACVF is located toward the southeast end of Great Xing'an Range (also known as Da Hinggan Mountains; both names are legitimate, but this paper utilizes the name as Great Xing'an Range). The highest ridges in ACVF are nearly 1500 m above sea level. The ACVF is located near the current political boundaries between China, Russia and Mongolia (**Figure 1**). The regional fault systems align NE–SW with the vents of ACVF, suggesting that the volcanic field is associated with major supracrustal weakness zones or even be linked to rifting and/or reactivation of Mesozoic structural zones separating major tectonic terrains (**Figures 1 and 2**). The rifting history of the region occurred in two major phases [12] around the Songliao Graben (**Figure 1**). It is believed that Songliao Graben subsidence is related delamination of the lithosphere and thinning of the upper crust of NE. China [12–15]. One of the conventional concepts is that the ascending asthenosphere caused by subduction of the down-going slab into the upper mantle initiated and sustained the delamination processes that were manifest as rifting in NE. China [1]. ACVF is located on the west flank of Songliao Graben (**Figure 1**). Hence the regional tectonic setting, characterized by the fault-controlled features, resulted fissures and NE-SW orientation and alignment of vents of (**Figure 2**). These are correlated with macro scale the tectonics of NE

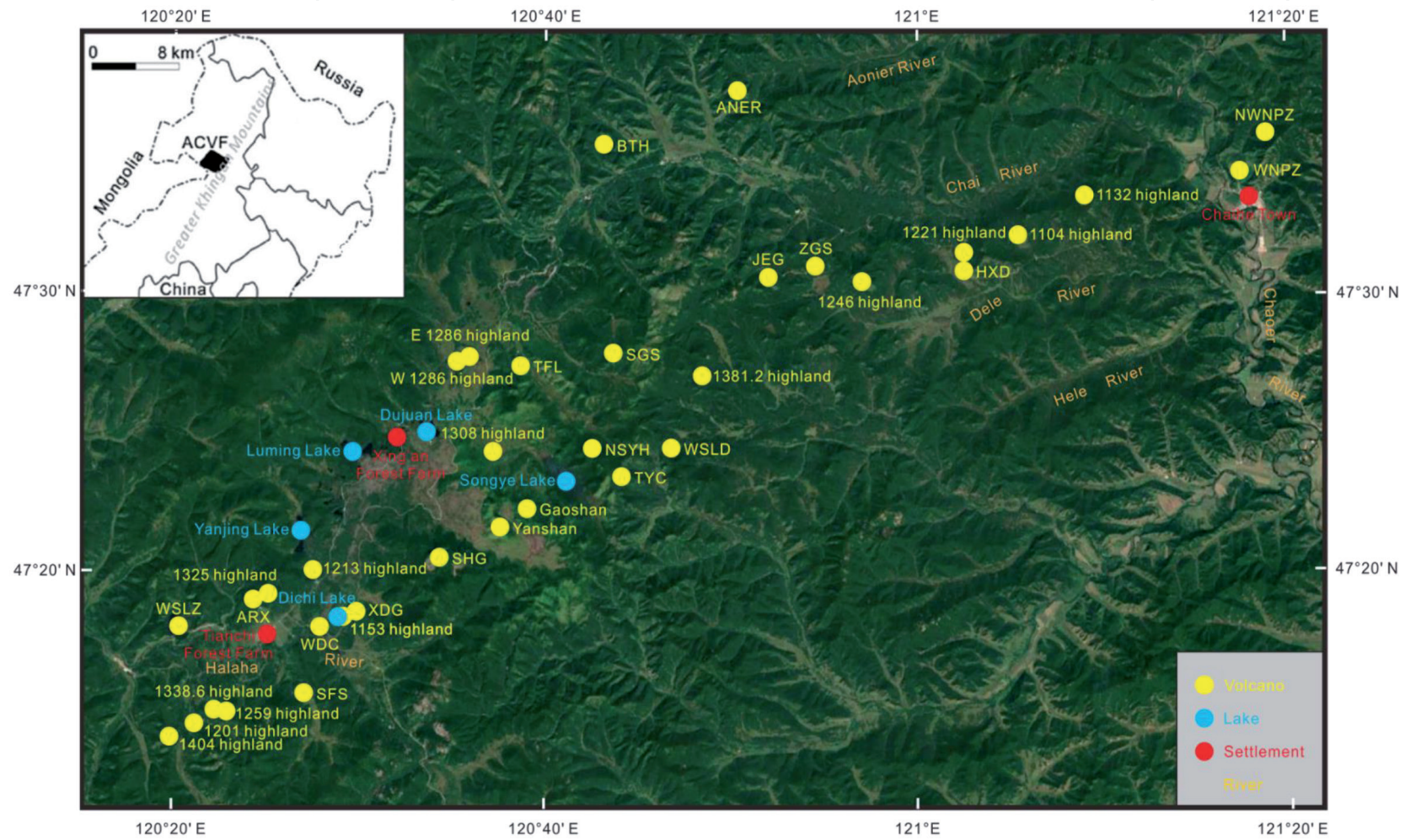


**Figure 3.**

A GoogleEarth map showing the volcanic locations from where basic volcanological information is available. The names and abbreviations also correspond to the common name the locations entered to various publications.

China. Volcanoes of ACVF overlie from Mesozoic basement rocks, such as granites and metamorphosed sediments [16–20]. The eruptive products are interfingering with various Quaternary sediments that accumulated in intra-mountain basins and along fault-controlled valley networks (**Figure 2**). The granitoid basement is strongly fractured, intruded by younger mafic to intermediate dyke swarms and usually covered by thick surface material derived from erosion and in situ weathering. Basement rocks are abundant in pyroclastic rocks as accidental lithics, especially those formed during explosive magma and water interaction. These lithics are preserved as xenoliths in individual or cored bombs in pyroclastic breccias or as accidental lithics of ash and lapilli in pyroclastic density current (PDC) deposits and within lava flows. Among the country-rock debris, there are low-grade metamorphic rocks or meta-sediments (commonly referred informally as “mudrocks”) in minor amounts within the pyroclastic beds. These rocks are also part of the Late Mesozoic basement assemblages.

The region around ACVF includes two main fluvial systems (Halaha River and Chaoer River) and several lacustrine systems (**Figures 2 and 3**). The lacustrine systems likely been formed after major lava flows diverted the fluvial channels. For example, a lake formed when a lava flow from the Yanshan – Gaoshan volcanic systems blocked the Halaha River approximately 2000 years ago (**Figures 2 and 3**) [11]. Major structural zones facilitated the storage of groundwater that was driven downward to the lowlands where springs and/or channels developed between major lava flow units [1, 21].

Annual precipitation is about 450 mm; the average temperature is around  $-2.7^{\circ}\text{C}$  in the range of  $-25.1^{\circ}\text{C}$  in January to  $16.8^{\circ}\text{C}$  in July with about six months of the year below  $0^{\circ}\text{C}$ . These data indicate that ACVF lies within typical subarctic conditions with a strong monsoonal influence [22]. Data relating to paleo-monsoon conditions in NE China are rarely found. However, research based on the lacustrine sediments found in the bottom of crater lakes in ACVF show that around the Last Glacial Maximum (LGM), about 18,000 BP, there was a significant enlargement of the northern grassland areas and warm periods are recorded during mid-Holocene (10000–6000 BP) [21]. These stages were influenced by the East Asian Monsoon. More recently the areas in forest are enlarging; this might indicate influence from the warm periods of mid-Holocene [21]. The present region is covered by typical subarctic forest (*Betula*), grass and shrubland. Volcanic landforms are heavily vegetated, and large and continuous exposures are rare, making geological mapping challenging. Soil formation is intense and even a seemingly young volcanic landforms are covered by thick Holocene sediments or typical sub-arctic mass-movement generated cover beds. The sub-arctic environments and high latitude lead to frozen ground for half the year (Oct to Apr) and only five months when the ground is not frozen (mid-Apr to Sep). A major wildfire in 1987, the Black Dragon fire event, caused widespread destruction of the vegetation around Yanshan-Triple Vent and Gaoshan. Nowadays, that area of forest and vegetation are regenerating and nearly cover the volcanic sites. This means that during field trips some of the areas cannot be assessed and observed.

### **3. Arxan-Chaihe volcanic field**

The Arxan-Chaihe Volcanic Field (ACVF) is recognized as a monogenetic volcanic field covering an area nearly 2000 km<sup>2</sup> [9, 10, 23]. Within this area, at least 47 vents have been identified so far; however, this is likely a minimum number [9]. ACVF has been experiencing high erosion triggered by dramatic temperature changes and fluctuating surface water runoff. Two major fluvial systems within ACVF, the Halaha

River and Chaoer River, facilitate surface erosions (**Figures 2** and **3**). They rework the volcanic materials and modify the general topography. Within ACVF volcanic landforms typical of a monogenetic volcanic field, such as tuff rings, scoria/cinder cones, fissures, lava flows, as well as ponded lava flows, have been recognized [9, 10]. This great diversity of monogenetic volcanic landforms gives the region its high geoheritage value and was the basis for protecting of volcanic landforms by the establishment of a geopark network in the region through intensive work since 2004. The western side of the ACVF became part of the UNESCO Global Geopark Network in 2017 (<http://www.unesco.org/new/en/natural-sciences/environment/earth-sciences/unesco-global-geoparks/list-of-unesco-global-geoparks/china/arxan/>). The recognition of the region's volcanic geoheritage in the highest level shows the importance of the ACVF as an intraplate volcanic field that is far from active plate margin processes and still recognized as an active volcanic region [9]. The ACVF is one of the lesser known volcanic regions of the world, and its physical volcanology and the implications to potential volcanic hazard have not yet been studied extensively.

#### 4. Vent locations and volcano morphology

So far, ACVF preserves at least 47 (known) vents in a 2000 km<sup>2</sup> area (**Figure 2**). From these 47 vents, only 35 were investigated in more detail and assigned to some volcanic geofoms (**Figure 3**, and **Table 1**). The age of the volcanoes were mostly assigned by their relative stratigraphy (**Table 1**) as sporadic and random absolute age dates are available [10, 24–26] only from a handful of identified volcanoes (**Table 2**). As absolute age dating using radiometric tools such as K-Ar or Ar-Ar methods are problematic in young mafic volcanics, most of the data derived from lava flows and coherent lava as pyroclasts from volcanic edifices. Lava flows however shows that volcanism was spread through time in the wider ACVF region (**Table 2**). This means that the available age data should be viewed with care and many data may not representative for an eruption age of the volcano located in the vicinity of the sampling point but shows ages of earlier lava flows. The volcanic landforms identified in ACVF include tuff rings, scoria/spatter cones, complex volcanic cones and tumuli structures, respectively (**Figure 4**). Tongxin Volcano (**Figure 4A**), is the largest tuff ring preserved in the ACVF with a rim to rim diameter of 1.4–1.1 km. The volcanic edifice is sandwiched between cliffs of basement rock (granite and metavolcanics) forming a typical intramountain basin that has been gradually filled from the north by an alluvial fan (**Figure 4A**). Bedrock is exposed about 306 m above the present-day crater lake surface that is commonly flanked with debris. The average elevation of the ring boundary is approximately 800 m above sea level. The central bottom of the lake is nearly flat with the present-day water depth of no more than 13 m.

The volcanic edifice itself is partially stripped off due to surficial erosion and the thickest tephra succession preserved in its western side is about 22 m thick. Due to thick soil cover (commonly over 2 meters thick, and impenetrable by manual trenching) and grass cover, the pyroclastic deposits associated with the former volcano commonly form only a thin drape of ash and lapilli. In well-protected areas in foothills, however, deposits have been identified over 10-meter thickness about 2–3 km away from the volcano. As preliminary field mapping showed, most of the deposits derived from Tongxin Volcano accumulated in a broad braided river system of the Chaoer River and post-eruptive fluvial processes are likely responsible for the removal of the erodible ash and lapilli.

There are no similar, large preserved tuff rings known from the ACVF, however, small phreatomagmatic volcanoes are suspected or been associated with the basal



Name on Figure 3	Formation Age	Location	Map view shape	Type of volcano or main eruptive product	Area of lava flow [km <sup>2</sup> ]	Main type of eruption	Relative height of edifice (m)
1 Gaoshan	Holocene	47°22'N, 120°39'E	Circular Horseshoe	Composite Cone	5	Violent Strombolian	362
2 Yanshan	Holocene	47°21'28"N, 120°37'30"E	Circular Horseshoe	Scoria Cone	50	Violent Strombolian	233
3 SHG	Holocene	47°20'28"N, 120°34'14"E	Circular Horseshoe	Scoria Cone	25	Strombolian	224
4 XDG	Holocene	47°18'28"N, 120°29'40"E	Circular Horseshoe	Spatter Cone	5	Hawaiian	110
5 WNPZ	Late Pleistocene	47°34'13"N, 121°17'22"E	Circular	Maar With Tuff Ring, Base-Surge	7	Phreatomagmatic	198
6 WSLZ	Late Pleistocene	47°17'54"N, 120°20'10"E	Circular	Maar With Tuff Ring, Base-Surge	2	Phreatomagmatic	150
7 BTH	Late Pleistocene	47°35'18"N, 120°43'08"E	Ellipse	Tuff Ring, Base-Surge		Phreatomagmatic?	
8 ZGS	Late Pleistocene	47°30'52"N, 120°54'44"E	Long Horseshoe	Collapsed or Breached Scoria Cone	23	Strombolian	136
9 JEG	Middle Pleistocene	47°30'25"N, 120°52'00"E	Circular Horseshoe	Composite Cone	3	Strombolian	178
10 TFL	Middle Pleistocene	47°27'19"N, 120°38'36"E	Long Horseshoe	Composite Cone	12	Strombolian and Phreatomagmatic	170
11 SGS	Middle Pleistocene	47°27'51"N, 120°43'34"E	Long Horseshoe	Collapsed or Breached Scoria Cone	12	Strombolian	168
12 TYC	Middle Pleistocene	47°23'23"N, 120°44'00"E	Circular Horseshoe	Composite Cone	11	Strombolian	122
13 1104 highland	Middle Pleistocene	47°32'2"N, 121°5'00"E	Circular Horseshoe	Composite Cone	20	Strombolian	154

Name on Figure 3	Formation Age	Location	Map view shape	Type of volcano or main eruptive product	Area of lava flow [km <sup>2</sup> ]	Main type of eruption	Relative height of edifice (m)
14 1132 highland	Middle Pleistocene	47°33'00"N, 121°9'20"E	Circular Horseshoe	Composite Cone	10	Strombolian	182
15 ANER	Middle Pleistocene	47°37'17"N, 120°50'30"E	Circular Horseshoe	Composite Cone	25	Strombolian	172
16 NWNPZ	Middle Pleistocene	47°35'35"N, 121°19'00"E	Circular Horseshoe	Spatter Cone	1	Hawaiian	205
17 1404 highland	Middle Pleistocene	47°14'8"N, 120°19'47"E	Circular Horseshoe	Collapsed or Breached Scoria Cone		Strombolian	254
18 1201 highland	Middle Pleistocene	47°14'31"N, 120°21'3"E	Long Horseshoe	Fissure Oriented Breached Scoria Cone		Hawaiian, Strombolian	50
19 WSLD	Middle Pleistocene	47°24'25"N, 120°46'49"E	Horseshoe	Collapsed or Breached Scoria Cone		Strombolian	50
20 SFS	Middle Pleistocene	47°15'45"N, 120°26'54"E	Horseshoe	Composite Cone	8	Strombolian	126
21 1153 highland	Middle Pleistocene	47°18'21"N, 120°29'4"E	Long Horseshoe	Fissure Oriented Breached Scoria Cone		Hawaiian, Strombolian	35
22 WDC	Middle Pleistocene	47°18'00"N, 120°27'50"E	Circular Horseshoe	Collapsed or Breached Scoria Cone		Strombolian	20
23 1213 highland	Middle Pleistocene	47°20'2"N, 120°27'27"E	Circular Horseshoe	Collapsed or Breached Scoria Cone		Strombolian	73
24 1308 highland	Middle Pleistocene	47°24'17"N, 120°37'8"E	Long Horseshoe	Collapsed or Breached Scoria Cone		Strombolian	38
25 1381.2 highland	Middle Pleistocene	47°26'53"N, 120°48'32"E	Circular Horseshoe	Collapsed or Breached Scoria Cone		Strombolian	131
26 1246 highland	Middle Pleistocene	47°30'18"N, 120°57'06"E	Circular Horseshoe	Collapsed or Breached Scoria Cone		Strombolian	196

Name on Figure 3	Formation Age	Location	Map view shape	Type of volcano or main eruptive product	Area of lava flow [km <sup>2</sup> ]	Main type of eruption	Relative height of edifice (m)
27 NSYH	Middle Pleistocene	47°24'23"N, 120°42'28"E	Circular Horseshoe	Collapsed or Breached Scoria Cone		Strombolian	66
28 1259 highland	Middle Pleistocene	47°14'56"N, 120°22'13"E	Circular Horseshoe	Collapsed or Breached Scoria Cone		Strombolian	60
29 1338.6 highland	Middle Pleistocene	47°14'56"N, 120°22'40"E	Circular Horseshoe	Collapsed or Breached Scoria Cone		Strombolian	138
30 W 1286 highland	Middle Pleistocene	47°27'30"N, 120°35'18"E	Horseshoe	Collapsed or Breached Scoria Cone		Strombolian	76
31 E 1286 highland	Middle Pleistocene	47°27'39"N, 120°35'49"E	Horseshoe	Collapsed or Breached Scoria Cone		Strombolian	45
32 1325 highland	Middle Pleistocene	47°19'09"N, 120°25'00"E	Horseshoe	Collapsed or Breached Scoria Cone		Strombolian	175
33 ARX	Middle Pleistocene	47°19'00"N, 120°24'16"E	Semi-Round	Scoria Cone	25	Strombolian	130
34 HXD	Middle Pleistocene	47°30'44"N, 121°2'35"E	Horseshoe	Composite Breached Scoria Cone	6	Strombolian	204
35 1221 highland	Middle Pleistocene	47°31'18"N, 121°3'32"E	Cone	Spatter Cone	8	Hawaiian, Strombolian	117

**Table 1.**

*Parameters for previously studied volcanoes in the ACVF.*

Sample No.	Location, Code (on Table 2) or Type	Dating method	Age	Reference
08AES02	WNPZ - 5	K-Ar	0.162 ± 0.02 Ma	Fan et al. [24]
07AES02	TFL - 10	K-Ar	0.246 ± 0.05 Ma	Fan et al. [24]
07CH04	Chaoer River – lava flow	K-Ar	0.269 ± 0.03 Ma	Fan et al. [24]
08AES09	WSLZ - 6	K-Ar	0.45 ± 0.03 Ma	Fan et al. [24]
08AES12	Budong River – lava flow	K-Ar	0.587 ± 0.06 Ma	Fan et al. [24]
07CH11	JEG - 9	K-Ar	0.743 ± 0.07 Ma	Fan et al. [24]
07CH09	Dele River – lava flow	K-Ar	1.365 ± 0.16 Ma	Fan et al. [24]
08AES04	TFL - 10	K-Ar	2.3 ± 0.06 Ma	Fan et al. [24]
08AES10	Budong River – lava flow	K-Ar	6.7 ± 0.18 Ma	Fan et al. [24]
Nt202	Tianchi forest farm – lava flow	K-Ar	0.34 ± 0.203 Ma	Liu et al. [25]
NW223	Wuchagou – lava flow	K-Ar	8.93 ± 0.64 Ma	Liu et al. [25]
NW214	Wuchagou – lava flow	K-Ar	9.94 ± 0.63 Ma	Liu et al. [25]
ARS002	TFL - 10	K-Ar	0.34 ± 0.03 Ma	Meng et al. [27]
ARS003	Dujuan Lake – lava flow	K-Ar	0.42 ± 0.10 Ma	Meng et al. [27]
ARS004	ARX - 33	K-Ar	0.53 ± 0.03 Ma	Meng et al. [27]
YL708	JEG - 9	tephra	14.2 ka	Sun et al. [26]
	Yanshan – 2 - under scoria fall	<sup>14</sup> C	1990 cal a BP	Bai et al. [11]
	Yanshan – 2 - under scoria fall	<sup>14</sup> C	1900 cal a BP	Bai et al. [11]

**Table 2.**

*Absolute dating results for the volcanic rocks of the ACFV [11, 24–26]. Samples marked as “lava flow” derived from extensive flow fields without exact information from their source vent.*

sections of large scoria cones. Tuofengling Lake (Camel Humps Lake in Chinese) is a good example for such volcano edifice architecture (**Figure 4B**). This volcano hosts an elongated lake suggesting that this volcano might be a complex volcano with multiple vents along the lake axis. This volcano appears different in its edifice architecture from Tongxin Volcano. In Tongxin Volcano, the country rocks are exposed in the inner basement hosting the crater lake while in Tuofengling, no basement is exposed. The volcanic edifice surrounding the crater lake is entirely volcanic in origin and part of a larger volcanic edifice. The preserved and accessible sites exposing typical lava spatter, agglomerate, scoriaceous deposits and various clastogenic lava flows suggest a largely magmatic explosive eruption style being responsible for the formation of them. However, from observations of the crater rim, at least two different volcanic deposits were found. The majority is typical of a scoria and spatter cone complex, while in the basal sections thick pyroclastic successions indicate explosive hydrovolcanism occurred as recorded by chilled pyroclast-dominated units predating the formation of the main central cones that were later disrupted giving space to form a broad and elongated crater within them (**Figure 4B**).

The youngest volcanic sites of the ACFV, i.e. approximately 2000 years ago [11], demonstrate a typical volcanic landform considered to be a common form of volcano types across the ACFV. Yanshan Hill marked as a single volcanic edifice, in

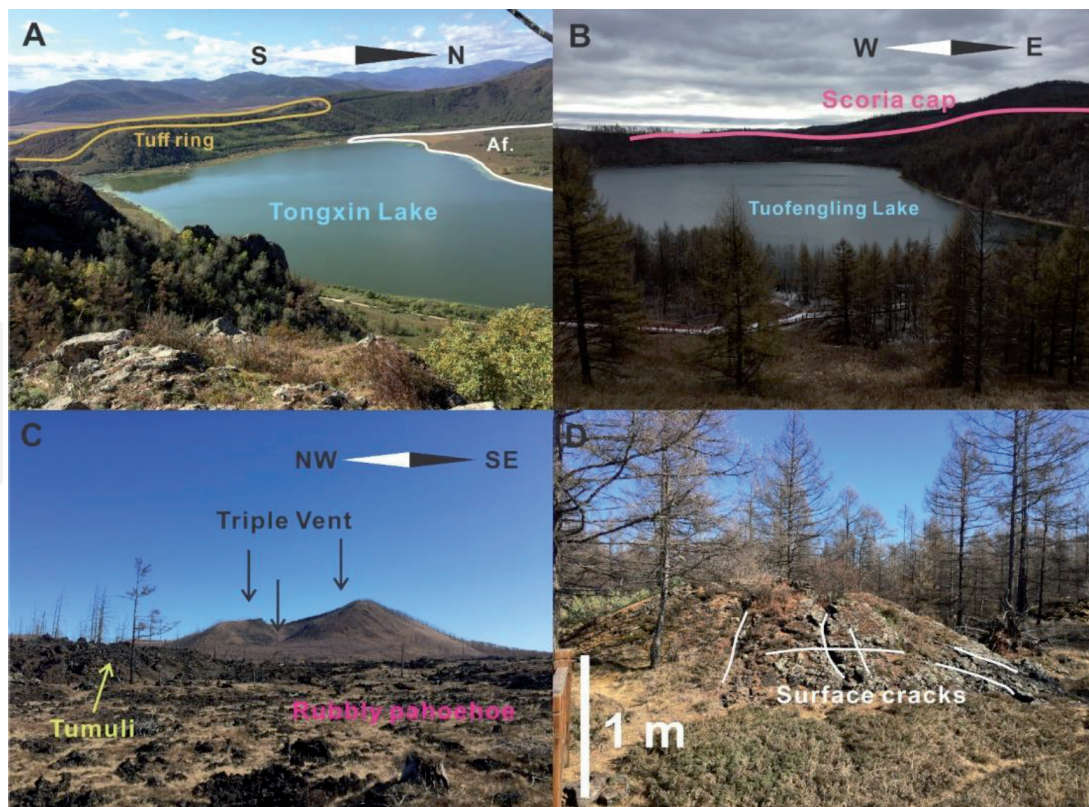


**Figure 4.** Four types of volcanic geoforms identified in ACVF, such as (A) tuff ring; (B) complex cone; (C) scoria/cinder cone; (D) tumuli.

fact, consists of at least three preserved volcanoes, informally named as the Triple Vent forming a volcanic complex. This volcano is a nested and closely spaced scoria cone edifice (**Figure 4C**). The main edifice is a steep-sided scoria cone with slope angles about  $45^\circ$ . The elevation of this volcano is about 1590 m above sea level. The volcanic complex was the source of extensive lava flows that reached 4 km to the west and captured the Halaha River causing major landscape modification and damming of the fluvial system. The lava flows show inflation and deflation features, development of pressure ridges, tumuli and outbreaks leading to the formation of a complex laterally changing surface flow morphologies ranging from rubble pahoehoe to aa lava morphotypes. Such large and complex volcanoes are the main volcanic landforms along with the main structurally controlled vents and with NE-SW trending structural elements. The complexity and estimated edifice volumes, as well as the large volume of associated lava flows of these volcanoes, suggest these eruptions changed the actual erupting points within km-ranges, were likely long-lasting events and were capable for sustained eruptions such as sub-Plinian or violent Strombolian style eruptions. This is supported by the extensive ash plain mapped around Yanshan.

Across the field, there is evidence of ponded lava flows, leaving behind a range of ponded lakes, clastogenic lava flows or agglomerates (**Figure 4D**). Based on the previous studies and evidence from 2019 fieldwork, the vents in ACVF are mostly fissure-controlled.

## 5. Evidence of explosive hydrovolcanism

Explosive hydrovolcanism is the result of magma and water explosive interactions [28]. Phreatomagmatism is a term reserved for magma and groundwater interaction commonly involving molten-coolant interaction [28]. In the ACVF,

pyroclast textures and deposit characteristics indicate that in low-lying areas, along fluvial valleys, phreatomagmatic explosive eruptions took place (**Figure 2**). While shreds of evidence of sustained phreatomagmatic explosive eruptions that formed maar or tuff ring volcanoes alone are not common, evidence of intermittent phreatomagmatic phases during eruptions are compelling. Evidence for phreatomagmatism can be seen in the form of quenched pyroclasts, glassy and angular texture of juvenile particles and relative abundance of country-rock fragments as accidental lithics in the pyroclastic successions. Indirectly, volcanic landforms may also be linked to the occurrence of phreatomagmatism in the course of volcanic eruptions; however, typical “wet”, phreatomagmatic landforms are rarely preserved at ACVF.

The most typical and complete site where evidence for explosive hydrovolcanism, phreatomagmatism has been identified in the ACVF is Tongxin Lake (**Figures 2 and 3**). Tongxin Lake has been recognized as a large tuff ring, partially draping over the rugged mountainous region (**Figure 2**). Two significant outcrops on the west flank of the ring margin have revealed deposits primarily formed by sustained phreatomagmatic eruptions. Dune-bedded, cross-stratified and wavy, accidental lithic-rich pyroclastic successions were observed and inferred to be the product of a combination of pyroclastic density currents and fallout. The succession of interbedded coarse-grained and fine-grained units suggest rapid changes in particle concentration, transportation style and interaction with microtopography. The majority of the pyroclasts are dense (i.e. low vesicularity), angular to subangular with delicate chilled margins. Accretionary lapilli are common in the fine ash beds.

Features indicative for phreatomagmatism can be found at other sites, such as Tuofengling/Camel Humps Lake, southwestern side of Tianchi/Heaven Lake, and in sporadic outcrops south of Wusulanzhi Lake (**Figure 2**). The deposits at Tuofengling Lake form a basal unit beneath the dominant scoria/cinder deposits. This unit is composed of a range of indurated parallel bedded, pyroclastic beds abundant in angular and dense lapilli within fine ash matrix. The average grain sizes from the deposits of Tuofengling is greater than the majority of the deposits recorded at Tongxin Lake (**Figure 5A**), and they are also more indurated than those from Tongxin Volcano.

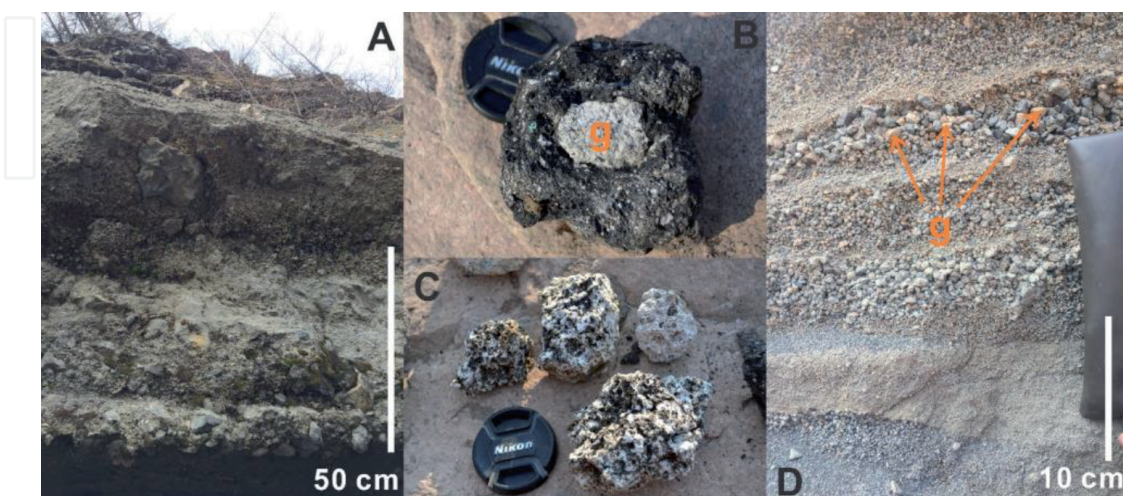


**Figure 5.** Typical pyroclastic deposit characteristics associated with explosive phreatomagmatic eruptions at the ACVF are linked to accidental lithic-rich pyroclastic breccias, inferred to be phreatomagmatic shower curtain deposits (A), the abundance of cored/laded (B) and partially melted accidental lithics in chilled lavas (C), and typical angular and low vesicularity juvenile pyroclasts forming typically graded beds in a combination of shower and pyroclastic density current-derived beds (D, captured on the south of Tongxin Lake, about 12 km away from the lake). Brown letter “g” indicates “granite”.

Bombs and accidental lithics in the eruptive products from Tongxin Volcano are commonly cored/loaded and/or granitoid lithics are fused or partially melted (**Figure 5B** and **C**). Cauliflower-shaped bombs with xenoliths are strong evidence for country-rock entrapment prior to the explosive disruption of the clasts during an eruption. Among the shell of the juvenile materials, large amounts of lithic debris are intercalated within. All these lithics are irregular-shaped, and, the juvenile materials are pasted onto the surface, chilled and form into the cauliflower-shaped bombs or juvenile pyroclasts. The general shape of those juvenile pyroclasts is sub-angular to angular. They probably came into contact with external water and became chilled, fragmented in brittle fashion to form angular, low vesicular pyroclasts. Pyroclastic successions, which are rich in accidental lithics and contain large volumes of chilled, angular juvenile pyroclasts commonly form unsorted, and graded beds intercalated with fine tuff that also contains accretionary lapilli (**Figure 5D**). These textural features and outcrop scale sedimentological characteristics are common among phreatomagmatic pyroclastic successions. Commonly, the fine-sized grains indicate the explosive phreatomagmatic fragmentation was accompanied by blasts; on the contrary, the coarse-grained and moderately sorted beds imply fallout origin.

## 6. Evidence of fissure-controlled volcanism

ACVF preserves a range of fissure-controlled vents (**Figure 2**). Those vents are always aligned NE-SW with the regional tectonic trend (**Figure 6**). Along with those fissures, several small craters with exposed fissures can be observed, for example Tianchi/Heaven Lake (**Figures 6** and **7**) and Dichi Lake (**Figure 8**). These two vent systems are not only the scenic spots of ACVF, but also, they preserve the typical topography and landforms of fissure-fed volcanoes.

Fissure eruption are common in monogenetic volcanic fields [29]. In ACVF, at least five distinct fissures can be identified from satellite images. They appear as linear ridge crests associated with closely spaced crater rows (**Figure 2**). In general ACVF eruptions occur along fissures formed by regional faulting systems [1];



**Figure 6.**

*Within Tianchi Lake, a shallow and elongated lake sitting well above the surrounding background topography suggesting the lake itself is a crater lake in a constructional volcanic landform such as a scoria cone. In both side (E and W) the elongated water-filled crater continuing into an elongated zone of depression surrounded by a spatter rampart (brown arrows). The overall orientation of the fissures is the same as the main structural setting of the ACVF (green arrow).*

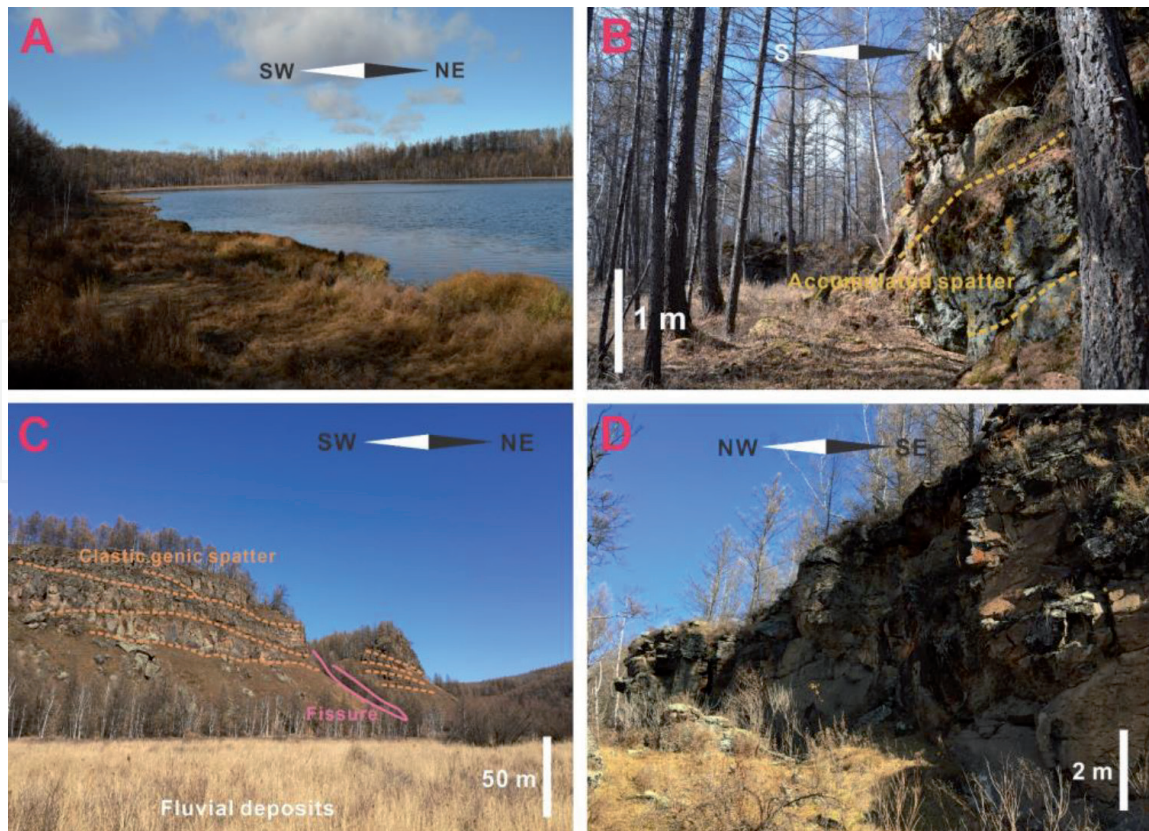


**Figure 7.** The field observations of Tianchi Lake (A) area showing spatter ramparts, clastogenic lava flows in the eastern (B) and western (C) regions of the Tianchi Lake. Platy lava flows also crop out more or less in the same elevation as the lake floor itself (D).

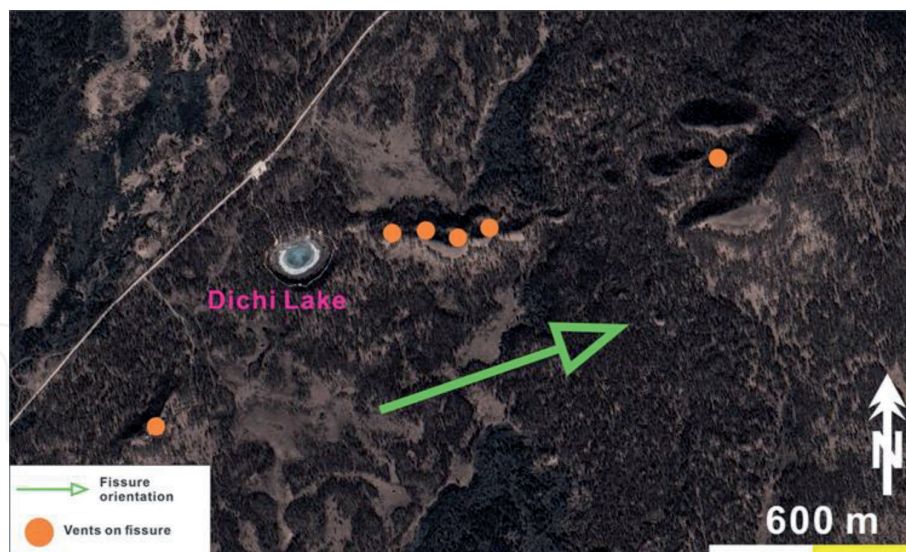


**Figure 8.** The GoogleEarth satellite image of the vicinity of Dichi Lake showing a chain of craters (brown dots) preserved oriented to the main structural zones of ACVF (green arrow).

however, the volcanoes have yet to be documented in detail. An elongated vent structure is apparent on a satellite view of Tianchi/Heaven Lake (Figure 6). The central part of the lake is bumped out through the surrounding topography, which indicates the presence of steep-sided and agglutinated scoria/cinder cone as the main volcano architecture in that area (Figure 6). A series of the lava flows with large amounts of scattered spatter deposits can be seen on the western side of the lake (Figure 6). The shape of the lake suggests an outpouring may have occurred on the southeast section



of the present-day water-filled, lacustrine basin (**Figure 7A**). Two other locations marking fissure structures on both sides of the lake, are shown by the large green arrow on **Figure 6**. The orientation of the fissures implies Tianchi Lake too follows the orientation of the regional structures (NE-SW). The brown dots on **Figure 6** indicate two rows of spatter and lava ramparts surrounding the margins of an eruptive fissure. This morphological setting and the presence of proximal spatter deposits, and clastogenic lava flows are interpreted to be the result of fissure eruptions that formed the Tianchi Lake Volcano. Also, the angle of repose of the main cone of Tianchi Lake Volcano is nearly 37–41 degrees suggesting a relatively young age of the volcano as Tianchi Lake Volcano is a scoria cone similar to other scoria cones in the world, i.e. the one in AVF (Auckland Volcanic Field) [30]. The total surface area of Tianchi Lake is approximately 0.1 km<sup>2</sup>, with about 1.2 km in its perimeter. The well-established forests and vegetation around the lake field observations and sampling difficult (**Figure 7A**). However, on the outer rim of the lake and the surrounding areas, volcanic materials are well-exposed and easily sampled.

Preliminary observations on the Tianchi Lake Volcano so far have been interpreted as it is a complex, elongated scoria cone. No phreatomagmatic deposits have been identified yet in the area suggesting that the volcano, despite it hosting a shallow lake, formed purely by magmatic explosive and effusive processes. During the dry season (August to October, annually), the height of the water level of the crater lake drops a few metres (**Figure 7A**). Along the eastern and western side of the preserved scoria cone, the fissure is marked by a 10 meters high wall of lava consisting of flows and spatter ramparts. Evidence of agglutinated interbeds within lava flows as well as some of clastogenic origin flows attests to fissure lava fountaining and shifting of active vent locations occurring. The surface structures of the fissure are similar to the lava flow, but are considerably harder, thereby preserving the original volcano architecture well. Occasionally, some lithic xenoliths (granite) can be observed within the spatter and lava flows. The rarity of vesicles in the lava flows and the agglutinated texture suggest the lava was degassed during the eruption, indicating that some sort of lava pool must have occupied the main axis of vents. On the western side of the main cone (**Figure 7C**), an approximately 50 m high wall of weakly stratified agglomerate and interbedded clastogenic lava flows formed due to explosive magmatic eruptions from a sustained lava fountaining stage forming a wall-like topography. In the middle part of the “wall”, a small gap between them might be the fissure structures aligning with the orientation. Field observations could only be taken from one side of the branch of the Halaha River. On the other side the bedded and agglutinated nature of the rocks are clearly visible suggesting the proximal location of the region. The horizontally stratified structures of the “wall” might indicate various stages of the cone building as well as the longevity of the eruptive phase. The thickness of the lava flows in the western side of the Tianchi/Heaven Lake is about 4–6 m (**Figure 7D**). The lava displays textures consistent with fluid transportation; there are also a moderate amount of bubbles. Within the bulk rock, some mafic minerals, including olivines and pyroxenes, can be seen. The top of these lava flow structures is eroded by the vegetation, but in some places the typical structures of aa type are still preserved.

Along with Tianchi/Heaven Lake, Dichi Lake is another small vent sitting on a fissure estimated to be about 3 km long. This lake might be the smallest one in ACVF (**Figure 8**). The green arrow on **Figure 8** marks the regional trend of the fissure orientation, which is also NE-SW, same orientation as Tianchi Lake. In comparison to Tianchi Lake, this fissure system is narrower but longer. The surrounding topography is flat without the tiny bumps due to local tumuli (**Figure 8**). Observations from the proximal areas of the Dichi Lake confirms the presence of pyroclastic breccias composed of dm-to-m sized angular blocks of lava commonly

forming well-defined zones several metres across. This deposit is estimated to be a few metres thick and sitting on a lava platform exposed in the crater wall of the Dichi Lake. There is no sign of deposits that may indicate PDC-generating eruptions or accumulation of typical base surge deposits. On the basis of this observation, Dichi Lake is likely a product of a short-lived, single explosive blast triggered by magma-water interaction along a fissure when the fissure hit the lowermost point of the region (**Figure 8**).

In the densely vegetated area of the Dichi Lake a volcanic cone chain (**Figure 9A**) with small preserved craters is still recognizable (**Figure 9B**). On the top of the small volcanic cones along the fissure, large blocks of scoria can be found hosting dm-sized spindle-shaped bombs (**Figure 9D**). The reddish color of most of the recovered bombs indicates high-temperature emplacement.

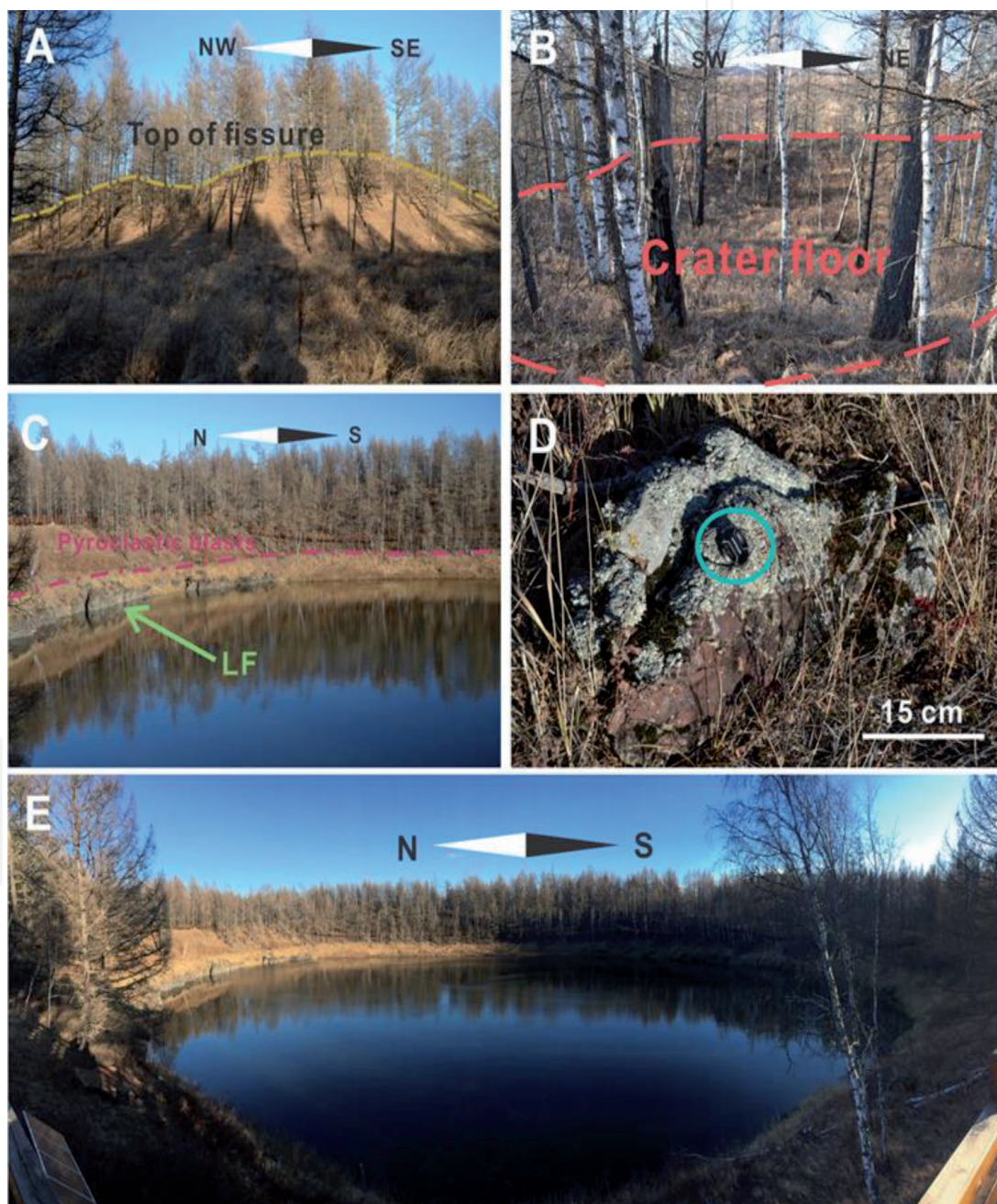


**Figure 9.** The field observations of Dichi Lake show small (tens of metres across) crater chains (a) with shallow but recognizable craters (B). In the crater wall of Dichi Lake lava flows exposed that are covered by pyroclastic breccia deposits (C). In the flank of the crater chains, fluidly shaped lava bombs suggest proximal portions of those areas (D). Dichi Lake best to interpret as a result of a single, short-lived phreatomagmatic blast (explosion crater) in the fissure edge.

## 7. Evidence of spatter-dominated volcanism

Spatter deposits are the typical dry eruption phase during the building of volcanic cones. In ACVF, spatter deposits are shown on the vents, which are scoria cones or fissure-related vents, such as Dichi Lake. However, one location preserves intact spatter deposits in the basal section of Tongxin Volcano (**Figure 10A**). The rest of the vents in ACVF only preserve scoria deposits from non-welded (black) to welded (red) varieties.

At Tongxin Volcano, the basal pyroclastic deposits along the western rim of the phreatomagmatic volcano preserve an about 2 m thick undulating, laterally discontinuous spatter unit (**Figure 10A**). On the top of the spatter unit, 30–50 cm of unsorted and laterally continuous PDC deposits were found suggesting dramatic eruption style change from a lava fountain stage to a phreatomagmatic blast eruption prior to the eruption becoming more sustained phreatomagmatic in style. Here the spatter deposits are in contact with the country-rock. Based on the contact relationships, Tongxin Volcano might have experienced an initial dry-eruptive phase followed by explosive phreatomagmatism. The distribution of the spatter deposits on Tongxin Volcano are elongated and expanded about 30 m long. On both ends of the spatter deposit, the thickness is thinner than the thickness on the middle part, and the shape is lens-like. Large accidental lithic bombs and blocks are commonly

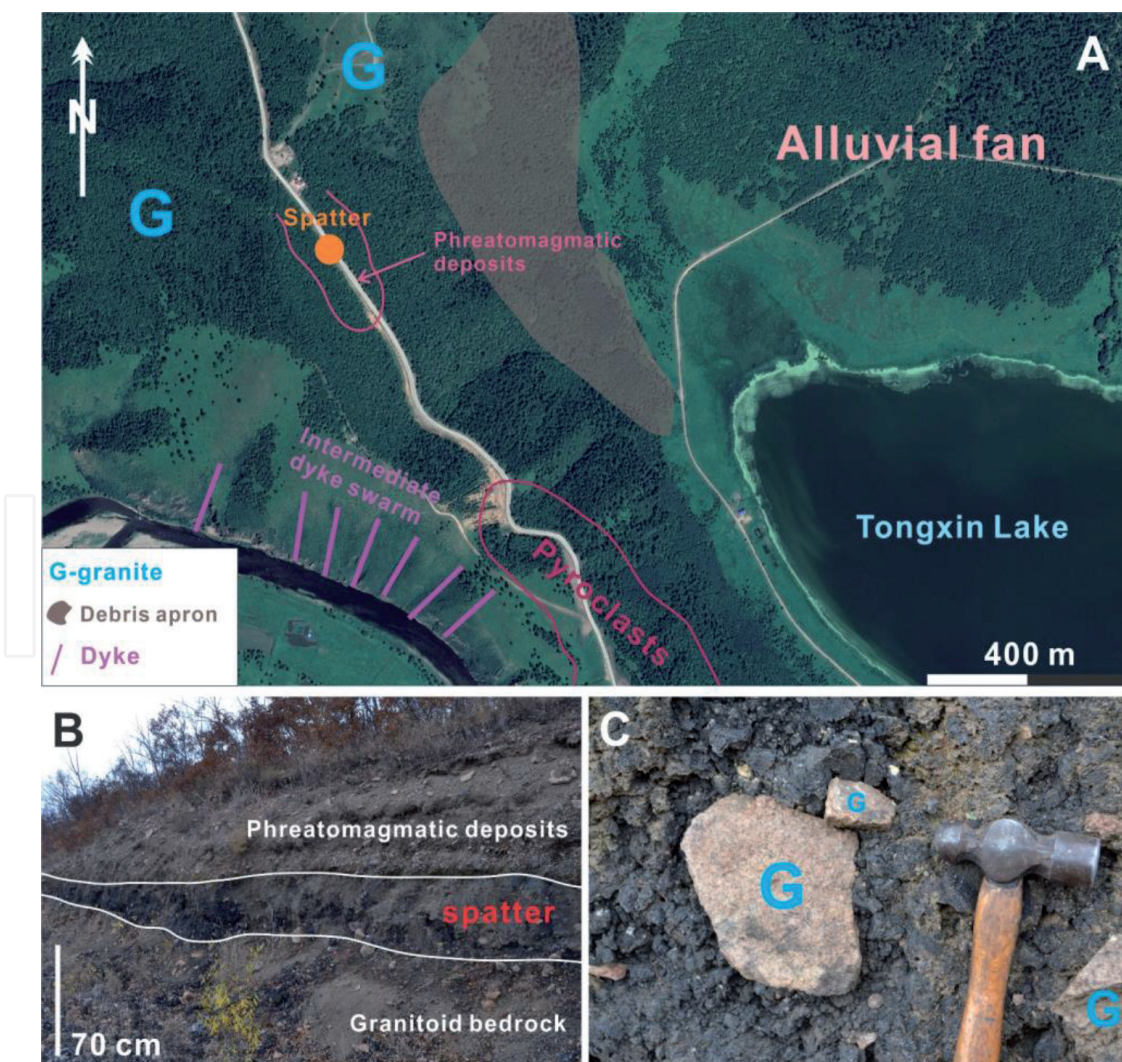


**Figure 10.** The spatters deposits on the northwestern side of Tongxin Lake (A). The blue letter “G” means “granite” for country-rocks. Spatter deposits lay on the bedrocks (B), and granitoid lithics commonly captured within the spatter deposit (C).

intercalated into the spatters suggesting some sort of excavation of the country-rock through the initial magmatic explosive phase of the Tongxin eruption. The weight of debris of the spatter is low due to the high vesicularity of the spatters. The spatter deposits are hardly found on other areas surrounding Tongxin Lake. However, at least two outcrops preserving the deposits in contact with bedrock indicate the dry-eruption phases, which are correlated with this spatter deposit.

Spatter beds are common elsewhere in the ACVF, especially along the previously described fissure aligned vents. Spatter deposits have also been recovered within exposed scoria cone sections indicating a switching on and off nature of the cone growing phases of those eruptions between Hawaiian and Strombolian style eruptions.

## 8. Evidence of lava-ponding in craters and topography lows

Lava ponding in ACVF is another feature characteristic of the volcanism in the region. The topography of the lava flows indicates an overwhelming dominance of various types of aa and rubbly pahoehoe lava flow morpho-types for the ACVF.

In ACVF, not only are small vents formed, but also, large craters formed that acted as traps for lava flows. In addition, lava commonly ponded in local basins or valley networks. A large crater (about 1.1 km across) from where one of the youngest and most extensive lava flows initiated to forms a significant volcanic landform with a typical volcanic morphology (**Figure 11**). The local name for this location as Dahei Gou, where it means “the big melanocratic valley”. Actually, there are two territories with the same name, but in considerations to the descriptions of volcanism of ACVF, the name “Dahei Gou” can only be a marker to define this unique location of ponded lava in a large crater. Dahei Gou Crater is located about 4.9 km northeast-ern of the three young volcanic cones of Yanshan (**Figure 11**). The satellite image (**Figures 2 and 11**) indicates that these two groups of vents (cones) have the same orientation as the Tianchi and Dichi fissures. Thus, it is believed there are at least two major regional structures controlling the vent distributions of ACVF.

The Dahei Gou crater is heavily vegetated, and only small tracks lead to the remote interior of a complex crater system. From the entrance of the valley,

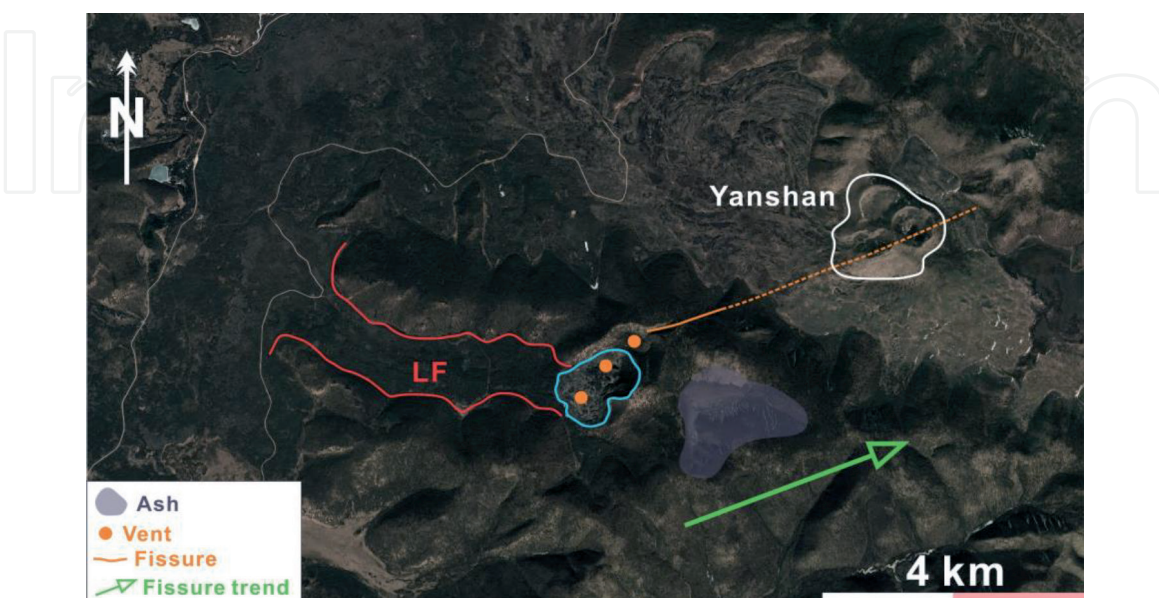


**Figure 11.** The satellite view of Dahei Gou (big Black Valley), also this photo depicts the relationship with Yanshan-triple vent. The dashed line indicates the extrapolation of the major fissure trend. The blue curve marks the caldera rim of Dahei Gou.

where the main lava flows spread along the Halaha River valley to the crater is about 4 km (**Figure 11**). The valley from the crater is filled with about 1 km wide lava flow along 4 km length, exposing typical flow margin features such as small to medium-sized tumuli and pressure ridges (**Figure 12A and B**).

Within the crater, a breakout zone can be identified along which the lava flow outpoured. In that area, rafted spatter sections and large slabs of lava in a randomly packed chaotic nature is evident. Inside the crater, individual tumuli, ramped up lava rubble and large piles of aa blocks form a rugged topography. Along the crater margin, lava flows preserve several meter-long cracks parallel with the crater margin (**Figure 12D**). These zones are interpreted as fractures along the inflated and ponded intra-crater where ponded lava collapsed upon the partial emptying of the large crater. The major body of the intra-crater lava flow is shown in **Figure 12C**. Along the crater margin, on the inner crater wall, drain back features can be seen that are partially collapsed back to the crater suggesting a dramatic outpouring event tapped the lava toward the valley. Dahe Gou is composed of at least three major nested crater systems, indicating vent migration, crater infill and sudden lava release forming a pit-like crater system. The total area of this crater is approximately 1 km<sup>2</sup>. The perimeter is about 4 km (**Figure 11**). Observations from the field indicate the presence of scoriaceous pyroclastic beds and agglomerate layers that formed due to explosive magmatic eruptions. On the eastern flank of the Dahe Gou, thick, black scoria ash drapes the landscape that has been partially down-cut by erosion (**Figure 11**). The textural similarities and the proximity of these ash plains to Yanshan deposits suggests that it might be part of the youngest eruptions of the Yanshan – Gaoshan volcanic system; however, this needs to be confirmed in future research.

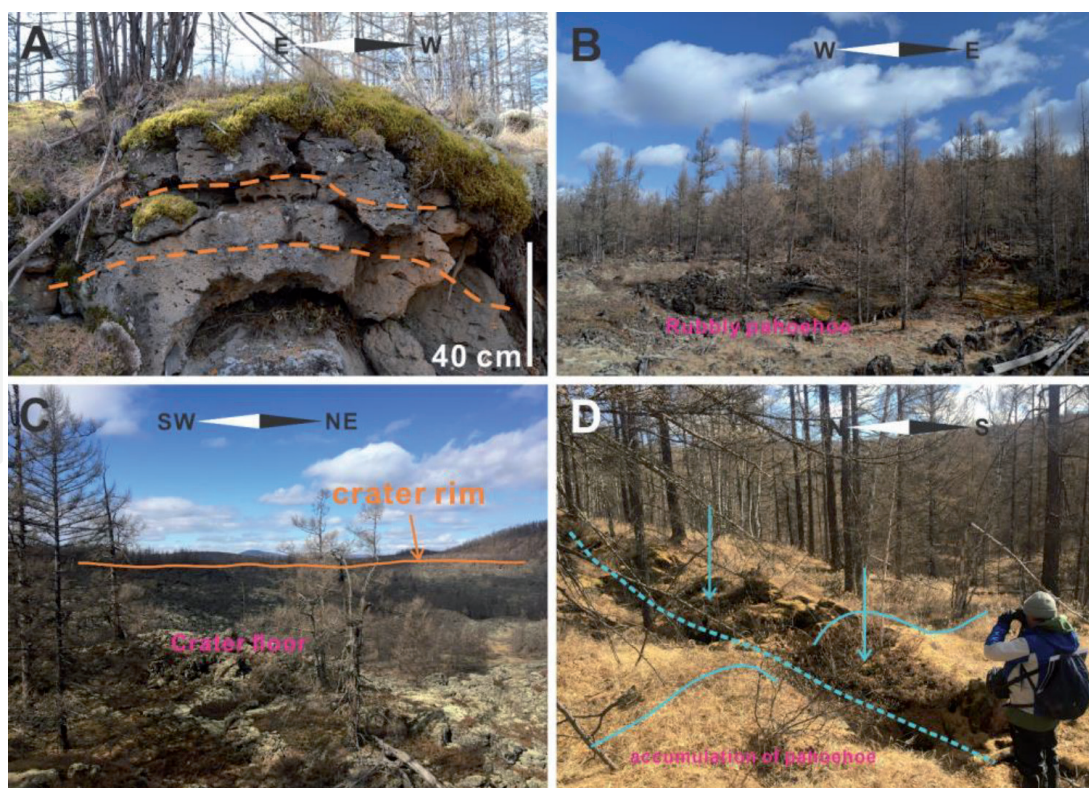


**Figure 12.**

*The major characteristics of Dahe Gou. Lava flows from the Dahe Gou shows pahoehoe surface textures in the lava fan regions with vesicles aligned following inflationary features (A), while deflationary features leaving behind collapsed lava tube roofs (B). The crater is filled with remaining parts of collapsed ponded lava zones, and along with the crater margins lava drawback features are prominent (C). Along the crater margins, margin-parallel cracks indicate collapse events (D).*

In the Arxan region, where lava flows are captured in the river valley, they form tumuli and lava tube networks that are partially collapsed, e.g. the fluvial areas of Halaha River. Such areas are prominent around the Wusulangzi Lake and Tianchi Lake (**Figure 13**). Eventually, in these areas, the lava flows are ponded around and form a range of significant landforms, some of them have already become the scenic spots for the volcanological educational purposes.

Along Halaha River large lava caves are partially open reaching a width of about 4 metres (**Figure 13A**). The lava flows formed successive layers with unambiguous and parallel boundaries. This suggests the flows ponded during several influx stages contemporaneously. The lava dripped from the ceiling (**Figure 13B**) but had no time on the ground consolidating while the processes were ongoing giving them a typical shape that is well preserved. Due to the roughness of the lava flow surface, the ponded lakes developed as the Halaha River became blocked (**Figure 13C**). The lake is no more than 6 m deep. Some of the ponded lakes have been misinterpreted as the sites of small cones; however, they are tumuli that formed along the flow margin. Cone and star shape tumuli displaying the cone shape forma group of dozens of tumuli in this region (**Figure 13D**). The cracks on the top of the tumuli indicate the upwelling and shape-forming processes were accompanied by tremendous volumes of steam. During the slow movement of lava flows, the gas and vaporized steam would occasionally gather and form large bubbles. Some of them were emitted through the surface of the flow. Thus, the inner parts of the tumuli are empty voids with a cone shape. In the Halaha River area, some tumuli are linear in shape (about 4 m in length and about 3 m in height) and align with each other. Most are similar size and volume.

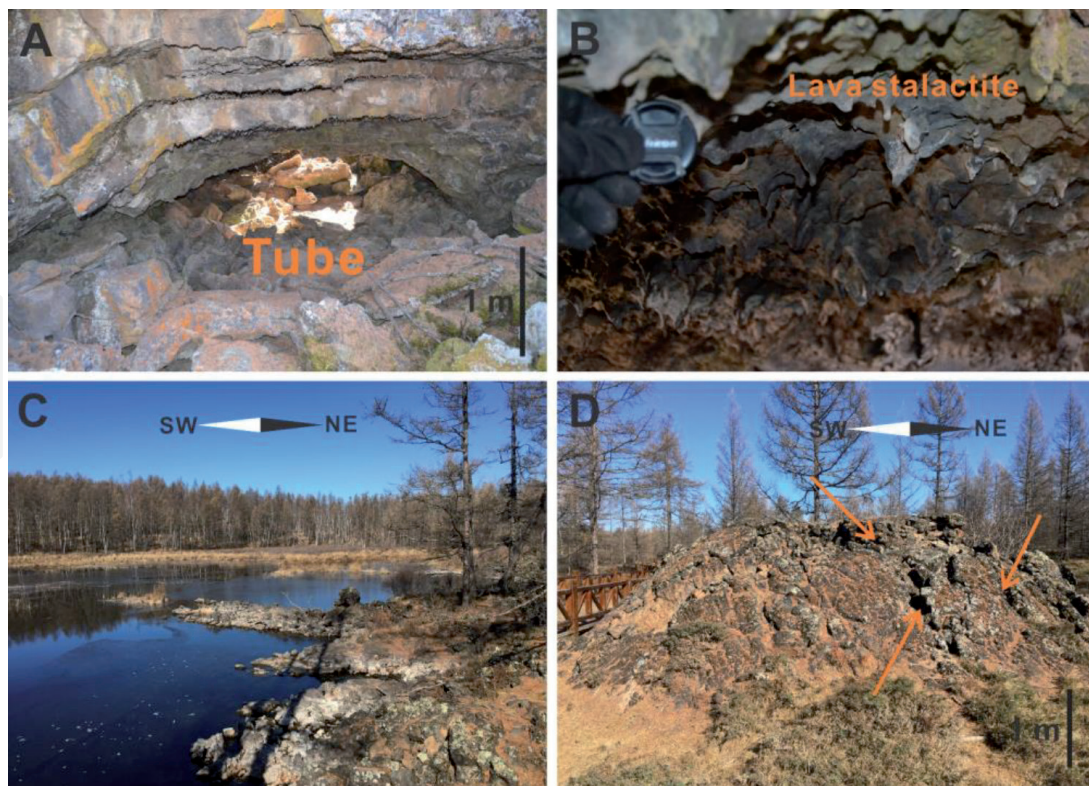


**Figure 13.** The ponded lava flow topography around fluvial areas of Halaha River exposes partially open lava tubes (A) that are draped by lava stalagmites (B). The blocked Halaha River forms a network of lakes and swamps (C). Tumuli are typically formed in the flat Halaha River valley where the cooling effect slowed down and eventually ponded the lava flows derived from the Dahei Goe volcano and Yanshan- Gaoshan volcanic system about 500 m above the valley floor (D).

## 9. Evidence of violent Strombolian style eruptions

Dry-eruption types of volcanism are the most common type of explosive volcanism in the ACVF. Large cones along the NE-SW trending ridge tops form a chain of cones that are vegetated and difficult to access. Most of these cones preserved edifice-building sections where ash, lapilli and bomb beds suggest normal Strombolian style volcanism. In the youngest known vent complex, the Gaoshan (High Hill) and Yanshan (Hill of Fire)-Triple vent large amounts of scoriaceous deposits form the cones and also spread across the landscape to form an extensive “ash plain” (**Figure 14**). The location of Gaoshan and Yanshan on the southeastern boundary of ACVF, is the location of several scoria cones representing the eruptive products of Strombolian style volcanism. In this section, Yanshan-Triple Vent form a more closely spaced vent system than those at Gaoshan inferred on the basis of the special distribution pattern of the volcanic products and the presence of multiple vents within one volcanic massif. The origins of Gaoshan are still being investigated.

Yanshan - Triple Vent, is located in the central part of ACVF (**Figure 2**). The highest peak in Yanshan is 1597 m above sea level. The total area of this “dry” hill is approximately 2 km<sup>2</sup>, with a perimeter of nearly 5.3 km. On every side of the hill, the burnt forests cover the slopes of the hill; this was a fire hazard at the end of 1987, i.e. Black Dragon fire.

As **Figure 14** shows, the lava flows cover most of the area surrounding Yanshan. The slope on the right side of the cone complex reaches 44° due to the welded nature of the proximal scoria beds. Slope angles are lower in the eastern side of the cone complex where a breached section of the cone formed the lava outpouring point from where a lava flow at least 3.77 km long flowed into the Halaha River valley. Some 5 km from the source, scoriaceous ash and lapilli formed at least 1 m thick units suggesting the youngest eruption products were dispersed widely. This dispersal pattern is suggestive of a violent Strombolian, or sub-Plinian stage of eruption during growth of the edifice complex.

Outlines of the ridge crests of the three vents can be pointed out from various observation points. Vent 1 is a flattened, shallow scoria ring structure (**Figure 14A and B**). In the crater rim crest, a scoria deposit can be reached beneath



**Figure 14.** The satellite view of Yanshan-triple vent. White lines mark the outlines of the three vents; red lines mark the outlines of the lava flow (LF). Yellow arrowheads show viewpoints from where **Figure 15A–C** was taken.

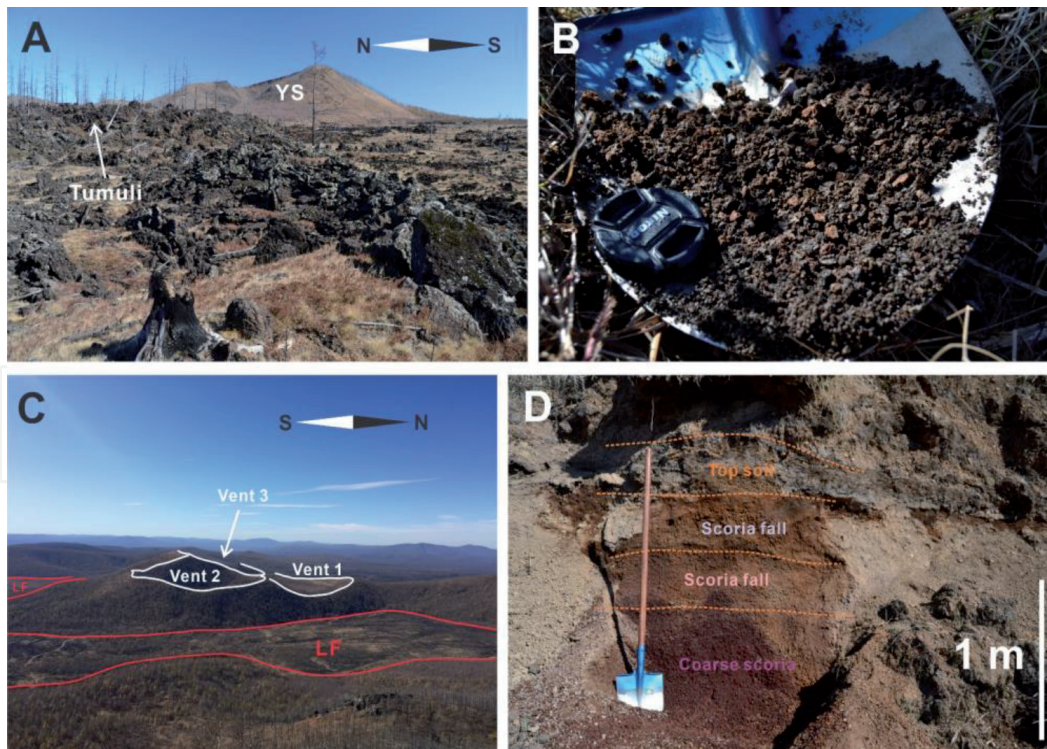


**Figure 15.**  
 The detailed the field observations of Yanshan-triple vent. A view from the south shows a complex cone and an open crater toward the west. Rubbly pahoehoe and tumuli around the cone form a rugged surface morphology (A). The surrounding area is covered by thick ash and lapilli blanket of black, and reddish scoria (B). At least three vents can be identified forming the Yanshan-triple vent as it can be seen from Gaoshan peak (C). The ash plain trench just about 2 km east of the vents shows multiple tephra layers indicating repeated and sustained eruptions (D).

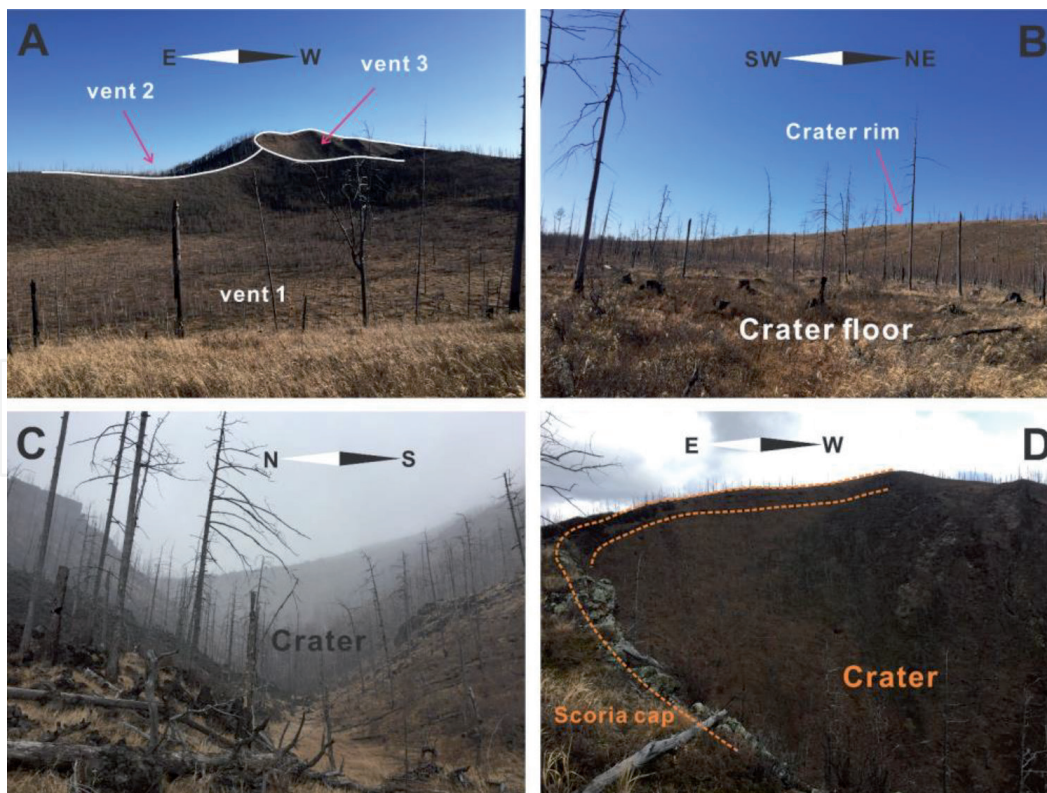


**Figure 16.**  
 Yanshan - triple vent field details. A photo that was taken from the western rim of the vent 1 showing the overgrowth of the vent 2 and 3 (A). The crater floor of vent 1 is filled with lava flow creating a rugged grass-covered morphology (B). Vent 3 is the source of the main lava flows outpoured from a breached section of the elongated (fissure-aligned) crater (C). The inner crater wall of the vent 3 exposes a set of agglomerates, welded scoria, spatter and localized clastogenic lava flows, all indicative for lava fountain dominated eruptions and intermittent more violent Strombolian phases (D).



a c. 50 cm thick soil. On vent 3, a clear crater wall collapse, and rafting from where the main lava flow escaped the crater are recorded (**Figure 16C**). The lava ponded in the crater and flowed out of the ring structures forming an outlet. The width of the breakage is narrow (**Figure 16C**), not more than about 250 m, which means the flux of the lava flows may reach a threshold value triggering the collapse of the edifice sector. The crater rim of the main crater composed of agglutinate, clastogenic lava and densely welded scoria beds (**Figure 16D**).

## 10. Discussion and comparison of ACVF to other similar volcanic fields elsewhere

The volcanism and volcanoes of ACVF were the subject of field work during 2018 and 2019. The observations made play a critical role in understanding the genesis, evolutionary history, types of landforms, and classification of topography. The observations made at ACVF are compared to several volcanic fields elsewhere in the world in terms of type and topography (**Table 3**).

1. The Crater of Moon, Idaho, USA, is an extensive volcanic field alongside the eastern bank of Snake River in the NE USA. It has about 25 cinder cones and large areas covered with the lava flows over an area of about 1600 km<sup>2</sup> [31–33]. In early research, this volcanic field was interpreted as a continental rift system, with c. 45 km long segment of the Great Rift. The lava flow morphotypes, the dominance of explosive magmatic eruptions over phreatomagmatic volcanism, and the type of monogenetic volcanoes made this field a good analogy with ACVF; however, the volcanoes of the Crater of Moon are smaller, less complex and closer spaced than those at ACVF.
2. The Laki fissure in Iceland is a fissure-driven volcanic cluster. Within it, there are two major vents, volcano Grímsvötn and volcano Thordarhryna, which represent the genesis of polygenetic volcanism. Significantly, the eruptions in 1783–1785 led to huge mortalities, famine, as well as the global temperature drop [34–36]. The Iceland volcanic fields belong to the Mid-Atlantic Ridge and the Greenland–Iceland–Faeroe Ridge, which are triggered by mantle plumes and formed North Atlantic Igneous Province. The fissure-controlled nature of the Laki eruption can be adopted as an analogy for the fissure-controlled volcano distribution in small and large scale at ACVF. The lava flow morphotypes, however, are more pahoehoe types, e.g. low viscosity melt, and make the lava flow fields of Laki appear different from those at ACVF.
3. Harrats of Saudi Arabia are clusters of the basaltic volcanic fields on the western coastal territories and part of the Red Sea Rift between the African and Arabian continental slabs. Harrat Rahat is one of the large Harrats among them. It is about 20,000 km<sup>2</sup>, and within it, there are approximately 500 individual vents radiating in every direction. The lava flows extend about 100 km to the west along the axis of the field [37, 38]. Harrat Rahat is a good analogy for ACVF in respect of the common large size of the volcanoes, complex volcano architecture, common features of ponding, inflation, deflation and occurrences of ponded lava within large craters and outside in flat-lying areas. Phreatomagmatism in Harrat Rahat has been recognized associated with the smallest volcanoes of the field [37]. The size of the field and the number of vents are also significantly larger to those recorded at ACVF [38].

Volcanic fields Ages	Rock Types	Tectonic Settings	Vent numbers Surface area	Volcano types
Arxan-Chaihe Volcanic Field (ACVF) Late-Pleistocene to Holocene	<b>Majority:</b> Basalt/Trachybasalt <b>Minority:</b> Basaltic Andesite	Intra- continental, rifting system	47+ 2000+ km <sup>2</sup>	Tuff rings, Scoria cones, Fissure vents, Caldera, Complex cones
Craters of Moon Idaho, USA Holocene	Basalt/Picro-Basalt, Trachybasalt/Tephrite Basanite, Trachyandesite/ Basaltic Trachyandesite	Rift zone, Continental crust (> 25 km)	25 1600 km <sup>2</sup>	Cinder cones, Fissure vents, Tuff rings
Laki Fissure, Iceland Holocene	Basalt / Picro-Basalt	Rift zone, Oceanic crust (< 15 km)	130 600 km <sup>2</sup>	Calderas, Craters, Fissure vents
Harrat Rahat Saudi Arabia Pliocene to Holocene	<b>Majority:</b> Basalt/Picro-Basalt, Trachybasalt/Tephrite Basanite, Trachyandesite/ Basaltic Trachyandesite <b>Minority:</b> Trachyte/ Trachydacite	Intraplate, Continental crust (> 25 km)	500 20,000 km <sup>2</sup>	Tuff cones, Tuff rings, Scoria cones, Lava domes
Chichinautzin Mexico Pleistocene to Holocene	<b>Majority:</b> Andesite/Basaltic Andesite, Trachyandesite/ Basaltic Trachyandesite, Dacite, Basalt/Picro-Basalt <b>Minority:</b> Trachybasalt/ Tephrite Basanite	Subduction zone, Continental crust (> 25 km)	220 6000 km <sup>2</sup>	Tuff cones, Scoria cones, Lava shields, tuff rings
Auckland Volcanic Field (AVF) New Zealand Late-Pleistocene to Holocene	Trachybasalt/Tephrite Basanite, Basalt	Subduction zone, Continental crust (> 25 km)	53 360 km <sup>2</sup>	Maars, Tuff rings, Lava shields, Scoria cones

**Table 3.**  
 Comparisons of ACVF to other volcanic fields [data from <https://volcano.si.edu>].

4. The Chichinautzin Monogenetic Volcanic Field is located on the central part of Mexico and belonged to Trans Mexican Volcanic Belt. There are more than 220 vents located within c. 6000 km<sup>2</sup> area. Most volcanoes in this field are basaltic andesite or basaltic trachyandesite [39–41]. Chichinautzin shares similarities to ACVF in respect to the similar individual volcano sizes, geochemistry, surface area and some aspects of forming nested vents and complex vent systems. However, Chichinautzin is a far more evolved complex and it is likely volcanoes were longer lived compared to those in ACVF where other than nested vent complex formation, the majority of its volcanoes are more typical of monogenetic volcanism.

## 11. Conclusion and volcanic eruption scenarios

Volcanism always cause a range of significant hazards to human societies. Not only to the life expectancy but they can also harm the foundations of infrastructures, exposed communities, disrupt the business, and put additional risks on the surrounding environments [42]. The hazards and threats from volcanic eruptions

and its related tectonic disasters are increasing annually to vulnerable societies. This is caused by the specific natural features of a volcanic field. The volcanic products, especially the mapped PDC deposits at Tongxin Volcano, can generate a range of very fertile soils and lands, which are utilized intensively for agriculture. However, the presence of thick and extensive PDC deposits indicate the threat of violent phreatomagmatic explosive events that can devastate large regions are ever present. On the other hand, the lava flows common at ACVF, which constitute the bulk of the volcanic products, are the very good construction materials. In general, the major effective regions under the shadows of volcanic eruptions are the proximal and intermediate areas, which can be impacted by the significant and severe threats from lava flows as well as deadly PDC flows.

In ACVF, several volcano types have been identified, but all of them show features of typical monogenetic volcanoes with small eruptive volume, small edifice size, typical deep sourced magma systems and suspected short eruption duration. The majority of the volcanoes identified formed through dry magmatic explosive eruptions forming lava spatter cones (**Figure 17A**), scoria cones (**Figure 17B**) or complex fissure aligned volcano chains (**Figure 17C**). These volcanoes pose hazards to their immediate surroundings; however, because we do not know where the next eruption will take place, they pose prediction uncertainty. The strong fissure alignments of the vents in hundreds of metres to tens of kilometers length, however, suggests that new vents likely will open along those main regional structure-controlled zones. The identification of fissure-fed, dominantly Hawaiian and Strombolian style eruptions suggests that once a new vent opens, the active vents likely will migrate along the fissure axis within the hundreds of metres to several kilometers length, making it difficult to mitigate the volcanic hazard. Due to the propagation of fissure through periods, volcanoes can be classified not only by type but also by eruption types. Generally, Strombolian eruptions, phreatomagmatic eruptions are the two major eruption types. Otherwise, the transition type or switching of the eruption types between two major eruptive behaviors is another major hazard event. It seems that phreatomagmatism occurred at ACVF (**Figure 17D**), but it is not the most significant type of volcanism. Phreatomagmatism seems to have occurred in low lying areas and/or along major fluvial networks. This style of volcanism formed a very violent event at Tongxin (**Figure 17D**). Similar eruptions in the fluvial valleys, where most of the human population lives today, could be catastrophic. It is also evident that the Tongxin eruption started just like any other volcanic eruption at ACVF, as lava fountaining along a migrating fissure (**Figure 17D1**). Once the rising magma along the fissure hit an active hydrogeological zone, violent phreatomagmatic explosions took place (**Figure 17D2**). Similar situations were suggested at Dichi Lake only on a significantly smaller scale. (**Figure 17E**) The nature of this eruption style transition accompanied by the fissure-fed nature of the volcanism needs further study to develop realistic eruptions scenario-based volcanic hazard study of the region.

Effects to the local topography are represented as the lava pouring into the fluvial systems changes the river flow patterns (**Figure 17F**). By damming rivers, temporary lakes can form changing the local hydrogeology that may promote explosive phreatomagmatism in the course of the ongoing eruption.

The lava ponding has also been recognized as an important process in the development of the lava fields. The complex high altitude volcanoes with multiple vents, shifting active vent locations and lava ponding in large craters are features that need to be considered in volcanic hazard eruption scenarios, as sudden collapse of scoria cone sectors and outpour of ponded lava could initiate large lava flows to areas that normally would not be considered as regions susceptible to lava flow hazards (**Figure 17G**).

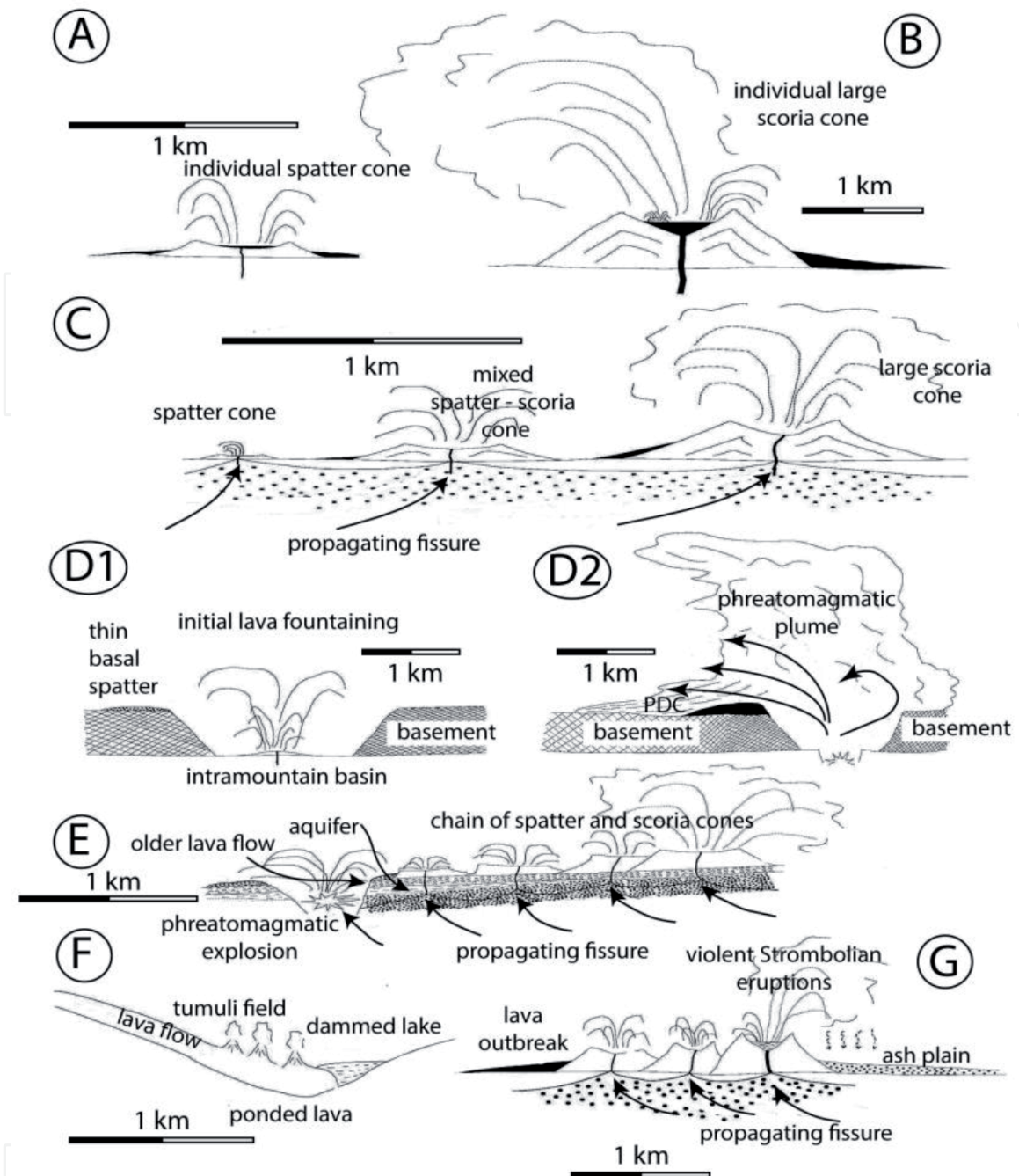


**Figure 17.** Typical volcano types identified at ACVF and their inferred schematic volcanic eruption scenarios. The ACVF has abundant individual lava spatter cones (A) and individual scoria cones (B) separated from other volcanoes by large (few kilometres) distances. More common volcano types of the ACVF are closely spaced spatter-and-scoria cone chains inferred to formed due to fissure-fed magmatic explosive eruptions (C). Phreatomagmatic volcanoes are rare at ACVF and their eruptive sequence commonly starts with a succession indicates initial magmatic explosive phases (D1) and thick laterally extensive pyroclastic density current (eg. base surge) deposited pyroclastic successions (D2). Occasionally, fissure-fed spatter-and-scoria cones terminate to a maar-forming eruption in low-land such as the Dichi Lake (E). Large-volume and long lava flows tend to dam syn-eruptive river network forming lakes where lava blisters such as tumuli field can form (F). Large and complex scoria cones in elevated ridges form multiple cone complexes, where outbreak of lava lakes can cause cone rafting and trigger sustained ash plumes to create ash and lapilli plains through violent-Strombolian style eruptions (G). Horizontal scales are approximate only.

## Acknowledgements

The authors wish to thank the support of the School of Agriculture and Environment, Massey University PhD Fellowship, the China – New Zealand Academic Exchange Program as part of the Royal Society of New Zealand Catalyst

Programme and the support from the Institute of the Geology and Geophysics of the Chinese academy of Sciences, Beijing. An earlier version of the manuscript was kindly reviewed by Dr. Gaby Gomez (U Morelia, Mexico) what for we are really thankful. Formal Anonymous reviewers' comments helped to elevate the quality of the chapter we thank for.

## **Funding**

This research was funded by the Massey University's Volcanic Risk Solution and School of Agriculture and Environment PhD-research fellowship. Fieldwork and logistics were supported by the Chinese Academy of Sciences and the Catalyst: Leaders New Zealand-China Scientist Exchange Programme.

## **Author details**


Boxin Li<sup>1</sup>, Károly Németh<sup>1\*</sup>, Julie Palmer<sup>1</sup>, Alan Palmer<sup>1</sup>, Jing Wu<sup>2</sup>, Jonathan Procter<sup>1</sup> and Jiaqi Liu<sup>2</sup>

1 Volcanic Risk Solutions, School of Agriculture and Environment, Massey University, Palmerston North, New Zealand

2 Institute of Geology and Geophysics, Chinese Academy of Sciences, Beijing, China

\*Address all correspondence to: k.nemeth@massey.ac.nz

## **IntechOpen**

© 2020 The Author(s). Licensee IntechOpen. This chapter is distributed under the terms of the Creative Commons Attribution License (<http://creativecommons.org/licenses/by/3.0>), which permits unrestricted use, distribution, and reproduction in any medium, provided the original work is properly cited. 

## References

- [1] Liu, J.Q., J.T. Han, & W.S. Fyfe, (2001). Cenozoic episodic volcanism and continental rifting in northeast China and possible link to Japan Sea development as revealed from K-Ar geochronology. *Tectonophysics*. 339(3-4): 385-401.
- [2] Wu, J., Z. Zhu, C. Sun, P. Rioual, G. Chu, & J. Liu, (2019). The significance of maar volcanoes for palaeoclimatic studies in China. *Journal of Volcanology and Geothermal Research*. 383: 2-15.
- [3] Sun, C., K. Nemeth, T. Zhan, H. You, G. Chu, & J. Liu, (2019). Tephra evidence for the most recent eruption of Laoheishan volcano, Wudalianchi volcanic field, northeast China. *Journal of Volcanology and Geothermal Research*. 383: 103-111.
- [4] Ramos, F.C., J.A. Wolff, J.E. Buettner, H.Q. Wei, & J. Xu, (2019). Ra/Th ages of sanidine in young trachytes erupted at Changbaishan Volcano, China. *Journal of Volcanology and Geothermal Research*. 374: 226-241.
- [5] Pan, B., S.L. de Silva, J. Xu, Z. Chen, D.P. Miggins, & H. Wei, (2017). The VEI-7 Millennium eruption, Changbaishan-Tianchi volcano, China/DPRK: New field, petrological, and chemical constraints on stratigraphy, volcanology, and magma dynamics. *Journal of Volcanology and Geothermal Research*. 343: 45-59.
- [6] Wei, H., G. Liu, & J. Gill, (2013). Review of eruptive activity at Tianchi volcano, Changbaishan, northeast China: implications for possible future eruptions. *Bulletin of Volcanology*. 75(4).
- [7] Xiao, L. & C.Z. Wang, (2009). Geologic features of Wudalianchi volcanic field, northeastern China: Implications for Martian volcanology. *Planetary And Space Science*. 57(5-6): 685-698.
- [8] Feng, M. & J.L. Whitford-Stark, (1986). The 1719-1721 eruptions of potassium-rich lavas at Wudalianchi, China. *Journal of Volcanology and Geothermal Research*. 30: 131-148.
- [9] Németh, K., J. Wu, C. Sun, & J. Liu, (2017). Update on the Volcanic Geoheritage Values of the Pliocene to Quaternary Arxan-Chaihe Volcanic Field, Inner Mongolia, China. *Geoheritage*. 9(3): 279-297.
- [10] Wang, L., M. Tian, X. Wen, L. Zhao, J. Song, M. Sun, H. Wang, Y. Lan, & M. Sun, (2014). Geoconservation and geotourism in Arxan-Chaihe Volcano Area, Inner Mongolia, China. *Quaternary International*. 349: 384-391.
- [11] Bai, Z., M. Tian, F. Wu, D. Xu, & T. Li, (2005). Yanshan, Gaoshan - Two active volcanoes of the volcanic cluster in Arshan, Inner Mongolia. *Earthquake Research in China*. 21(1): 113-117.
- [12] Liu, J., (1989). On the origin and evolution of continental rift system in Northeast China. *Chinese Journal of Geology*. 3: 209-319.
- [13] Jia, H., H. Ji, L. Wang, D. Yang, P. Meng, & C. Shi, (2016). Tectono-sedimentary and hydrocarbon potential analysis of rift-related successions in the Dehui Depression, Songliao Basin, Northeastern China. *Marine and Petroleum Geology*. 76: 262-278.
- [14] Gao, Y.-G. & Y.-H. Li, (2014). Crustal thickness and V-p/V-s in the Northeast China-North China region and its geological implication. *Chinese Journal of Geophysics-Chinese Edition*. 57(3): 847-857.
- [15] Zheng, Y., W. Shen, L. Zhou, Y. Yang, Z. Xie, & M.H. Ritzwoller, (2011). Crust and uppermost mantle beneath the North China Craton, northeastern China, and the Sea of Japan from

ambient noise tomography. *Journal of Geophysical Research-Solid Earth*. 116.

[16] Zhang, C., J.-Y. Quan, Y.-J. Zhang, Z.-H. Liu, W. Li, Y. Wang, C. Qian, L. Zhang, & J.-T. Ge, (2020). Late Mesozoic tectonic evolution of the southern Great Xing'an Range, NE China: Evidence from whole-rock geochemistry, and zircon U-Pb ages and Hf isotopes from volcanic rocks. *Lithos*. 362.

[17] Liu, Y., S.-H. Jiang, L. Bagas, C.-L. Chen, N. Han, & Y.-Y. Wan, (2020). Petrogenesis and metallogenic potential of the Wulanba granite, southern Great Xing'an Range, NE China: constraints from whole-rock and apatite geochemistry. *Geological Magazine*. 157(3): 411-434.

[18] Wan, L., C. Lu, Z. Zeng, A.S. Mohammed, Z. Liu, Q. Dai, & K. Chen, (2019). Nature and significance of the late Mesozoic granitoids in the southern Great Xing'an range, eastern Central Asian Orogenic Belt. *International Geology Review*. 61(5): 584-606.

[19] Ji, Z., W.-C. Ge, H. Yang, Q.-h. Wang, Y.-l. Zhang, Z.-h. Wang, & J.-H. Bi, (2018). Late Jurassic rhyolites from the Wuchagou region in the central Great Xing'an Range, NE China: Petrogenesis and tectonic implications. *Journal of Asian Earth Sciences*. 158: 381-397.

[20] Wang, T., L. Guo, L. Zhang, Q. Yang, J. Zhang, Y. Tong, & K. Ye, (2015). Timing and evolution of Jurassic-Cretaceous granitoid magmatism in the Mongol-Okhotsk belt and adjacent areas, NE Asia: Implications for transition from contractional crustal thickening to extensional thinning and geodynamic settings. *Journal of Asian Earth Sciences*. 97: 365-392.

[21] Zhao, C., X. Li, X. Zhou, K. Zhao, & Q. Yang, (2016). Holocene vegetation succession and responses to climate

change in the northern sector of Northeast China. *Science China Earth Sciences*. 46(1674-7240): 870.

[22] Liu, T. & Z. Ding, (1998). Chinese Loess and the Paleomonsoon. *Annual Review of Earth and Planetary Sciences*. 26: 111.

[23] Zhao, Y., Q. Fan, Z. Bai, Q. Sun, N. Li, J. Sui, & X. Du, (2008). Preliminary study on Quaternary volcanoes in the Halaha River and Chaoer River area in Da Hinggan Ling. *Yanshi Xuebao = Acta Petrologica Sinica*. 24(11): 2569-2575.

[24] Fan, Q., Y. Zhao, D. Li, Y. Wu, & D. Zheng, (2011). Studies on Quaternary volcanism stages of Halaha river and Chaoer river area in the Great Xing'an Range: Evidence from K-Ar dating and volcanic geology features. *Acta Petrologica Sinica*. 27(10): 2827-2832.

[25] Liu, J., (1987). Study on geochronology of the Cenozoic volcanic rocks in northeast China. *Acta Petrologica Sinica*. 6(2): 49-51.

[26] Sun, C., Q. Liu, J. Wu, K. Németh, L. Wang, Y. Zhao, G. Chu, & J. Liu, (2017). The first tephra evidence for a Late Glacial explosive volcanic eruption in the Arxan-Chaihe volcanic field (ACVF), northeast China. *Quaternary Geochronology*. 40: 109-119. S1871101416301558 [<http://dx.doi.org/10.1016/j.quageo.2016.10.003>].

[27] Meng F-c, Safonova I, Chen S-s, Rioual P (2018) Late Cenozoic intra-plate basalts of the Greater Khingan Range in NE China and Khangai Province in Central Mongolia. *Gondwana Research* 63:65-84

[28] Németh, K. & S. Kósik, (2020). Review of Explosive Hydrovolcanism. *Geosciences*. 10(2): 44.

[29] Kereszturi, G. & K. Németh, (2012). Monogenetic basaltic volcanoes: genetic classification, growth, geomorphology and degradation, K. Németh, Editor,

*Updates in Volcanology - New Advances in Understanding Volcanic Systems*, inTech Open: Rijeka, Croatia. p. 3-88 [<http://dx.doi.org/10.5772/51387>].

[30] Kereszturi, G. & K. Nemeth, (2016). Sedimentology, eruptive mechanism and facies architecture of basaltic scoria cones from the Auckland Volcanic Field (New Zealand). *Journal of Volcanology and Geothermal Research*. 324: 41-56.

[31] Leeman, W.P., C.J. Vitaliano, & M. Prinz, (1976). Evolved lavas from Snake-River Plain - Craters of Moon National Monument, Idaho. *Contributions to Mineralogy and Petrology*. 56(1): 35-60.

[32] Green, J. & N.M. Short, (2012). *Volcanic landforms and surface features: a photographic atlas and glossary*. Springer Science & Business Media.

[33] Greeley, R. & J.S. King, (1977). *Volcanism of the Eastern Snake River Plain, Idaho: A comparative planetary geology-guidebook*. National Aeronautics and Space Administration; 1st Edition (January 1, 1977) [ASIN : B000L7Z6NS]

[34] Thordarson, T., D.J. Miller, G. Larsen, S. Self, & H. Sigurdsson, (2001). New estimates of sulfur degassing and atmospheric mass-loading by the 934 AD Eldgja eruption, Iceland. *Journal Of Volcanology And Geothermal Research*. 108(1-4): 33-54.

[35] Thordarson, T. & S. Self, (1993). The Laki (Skaftár Fires) and Grímsvötn eruptions in 1783-1785. *Bulletin of Volcanology*. 55(4): 233-263.

[36] Thordarson, T. & S. Self, (2003). Atmospheric and environmental effects of the 1783-1784 Laki eruption: A review and reassessment. *Journal of Geophysical Research: Atmospheres*. 108(D1): AAC 7-1-AAC 7-29.

[37] Murcia, H., K. Németh, N.N. El-Masry, J.M. Lindsay, M.R.H. Moufti,

P. Wameyo, S.J. Cronin, I.E.M. Smith, & G. Kereszturi, (2015). The Al-Du'aythah volcanic cones, Al-Madinah City: implications for volcanic hazards in northern Harrat Rahat, Kingdom of Saudi Arabia. *Bulletin of Volcanology*. 77(6): 54.

[38] Murcia, H., K. Nemeth, M.R. Moufti, J.M. Lindsay, N. El-Masry, S.J. Cronin, A. Qaddah, & I.E.M. Smith, (2014). Late Holocene lava flow morphotypes of northern Harrat Rahat, Kingdom of Saudi Arabia; implications for the description of continental lava fields. *Journal of Asian Earth Sciences*. 84: 131-145.

[39] Nieto-Torres, A. & A.L. Martin Del Pozzo, (2019). Spatio-temporal hazard assessment of a monogenetic volcanic field, near México City. *Journal of Volcanology and Geothermal Research*. 371: 46-58.

[40] Nieto-Torres, A. & A.L. Martin Del Pozzo, (2019). Spatio-temporal hazard assessment of a monogenetic volcanic field, near Mexico City. *Journal of Volcanology and Geothermal Research*. 371: 46-58.

[41] Lorenzo-Merino, A., M.N. Guilbaud, & J. Roberge, (2018). The violent Strombolian eruption of 10 ka Pelado shield volcano, Sierra Chichinautzin, Central Mexico. *Bulletin of Volcanology*. 80(3).

[42] Blong, R.J., (1984). *Volcanic hazards. A sourcebook on the effects of eruptions*. Academic Press, Inc., Orlando, FL. Medium: X; Size: Pages: 427.